Department of Water Resources and Environmental Modeling
Faculty of Environmental Sciences
Czech University of Life Sciences Prague
Czech Republic

A novel methodology for green composite synthesis with the adsorptive application of aqueous organic contaminants

Presented by Nayan Kumar

Ph.D. Thesis

For the degree of

Doctor of Philosophy

February 2024

Under the supervision of

Marek Vach

Associate Professor

Czech University of Life Sciences Prague

ACKNOWLEDGEMENTS

I am expressing my heartiest gratitude to Prof. Marek Vach for giving me the opportunity to pursue my Ph.D. under his supervision, his trust, guidance, motivation and academic support, always helped me throughout my Ph.D. curriculum to give my best. The selection of research area was made more convenient for me by my supervisor for attaining the time bound results. I am grateful for his availability for the discussion regarding work progress and his extended assistance for the model fitting and equation derivation was really commendable.

I am highly obliged and thankful to Asst. Professor Vipin Kumar Saini, Doon University, Dehradun, for his extreme support for the resources offered for experimental set up in his lab and supervise the formal analysis, his proficiency in instrumentation really helped me in characterization techniques. I am grateful to him for teaching me the surface area analyzer and UV spectrophotometer analytical instruments, his advancement in adsorption techniques enriched my experimentation knowledge.

I am thankful for IGA and department head Prof. Martin Hanel for the financial grant during instrumental analysis. I also acknowledge the essential laboratory support by Environmental Geoscience lab and their cooperative staff for smooth cooperation for supporting experimental analysis.

The administrative staff Styblova Jana, Petra Kadlecova and Peter Basta for their extensive academic cooperation made the Ph.D. journey more organized and steady and immense technical support from IT department especially Aubrecht Jiri for his availability and quick response to any technical problems.

I would also like to thanks my colleagues for giving me healthy social environment and giving the warmth and affection of a family.

Finally, I would like to thank my parents, brother Ravi Kumar Sah and Brother -in- law Hemant Saini and his family for their affection and care for my work update and well being, specifically I mention my wife Kirti Saini and mother-in-law for supporting family with their love and care especially for kids (Ridhaan and Somil) as well as they supported me mentally and emotionally through all phases of highs and lows of research while achieving my Ph.D. goals.

ABSTRACT

The most common activation route for synthesizing the functional composite is chemical-based, which generates secondary pollutants and environmental toxicity. An absolute green methodology with no chemicals was designed with feedstock orange peel and eggshell. The two different methodology developed one method using the copyrolysis technique (Methodology I), where eggshell pyrolyzed with orange peel where as the other methodology used the eggshell in the form of suspension as the activating agent(Methodology II) . The methodology I was only optimized with response surface methodology .This novel approach induced natural activation during the pyrolysis process. The obtained composite with Methodology I was named EOC 300 and composite with Methodology II was named OPC9. The resultant composite was characterized with SEM-EDS, which showed the highly rich defect structure along with the regular compartment-like arrangement showed the tubular porous structure, whereas EDX analysis showed a rich percentage of Si along with enhanced K, Ca, Mg, Al, and P minerals over the surface. XRD patterns confirm the successful formation of the composite with the appearance of new peaks with increased intensities, and the sharpness of the peak showed a higher degree of crystallinity. The FTIR spectrum showed the new functional groups along with basic carbon skeleton structure resulting from high pyrolysis temperature. N2 adsorption-desorption isotherm provided a BET-surface area of 693 m^2/g for OPC9 and 64 m^2 /g for EOC300 with increased pore volume and an average pore diameter size of 0.6 nm, where predominant porosity was in the mesoporous range. The obtained composite application was utilized for the removal of organic contaminants , one of prominent oragnic contaminat was taken from dye industry named Methylene blue and other

was taken from emerging organic contaminants sector named Bisphenol-A. Both the composite showed excellent adsorption behavior for their respective contaminants . The composite EOC300 showed the maximum adsorption capacity of 167 m^2/g for Methylene blue where as composite OPC9 showed the great affinity towards Bisphenol A (BPA) with the 100% removal of the BPA and showed an maximum adsorption capacity of 159 mg/g. The adsorptive mechanism was well explained with the isotherm modeling and showed the balance of physiosorption, chemisorption, and pore diffusion; in addition, the kinetics of the adsorption was well explained with the pseudo-second-order reaction.

Keywords: Novel methodology; green activation; mesoporous; Orange composite; adsorption; Bisphenol A, Methylene blue.

CONTENTS

LIST OF FIGURES

List of Tables

Part I

Background

CHAPTER 1

Introduction

A comprehensive approach towards environmental issues is highly required for gaining ecological sustainability from the current perspective. Presently, the synthesis of engineered composite requires extensive use of chemicals for fabrication along with different layers of process, which mostly brings secondary pollutants to the surroundings. Whereas the environment in the existing situation demands more green techniques to reduce the secondary impact for achieving the sustainable development goal. Biochar and its composite have been extensively investigated in the past decades as a bio-sorbent for water and gas pollutants (Hong et al., 2021; Xue & Gao 2022; Anwar et al., 2022; Safarik et al., 2016; Yu et al., 2022; Dong et al., 2019). Moreover, the synthesis of biochar primarily involves biomass feedstock, whereas, biochar composite is the modified form of biochar, where biochar is used as the supporting carbon base for surface fabrication resulting in improved physical and chemical properties (Iqbal & Shah 2021; Zhang et al., 2022). Different precursors have been used to

prepare the base of the composite, primarily including lignocellulosic biomass such as agricultural waste (Kan et al., 2019; Poon et al., 2022, Ozsin et al., 2019), biological waste (Chen et al., 2022; Ok & Tsang 2017; Vithanage et al., 2019; Zhang et al., 2021), and keeping in consideration of circular economy, now most of the studies showed, raw materials such as food waste, sewage sludge, and other food processing organic waste to use as a biochar feedstock (Li et al., 2020; Alibardi et al., 2015; Nidheesh et al., 2021; Park et al., 2020; Lee & Ok 2020; Vo et al., 2022; Meili et al., 2022; Jaiswal et al., 2016). Amongst different processes, the co-pyrolysis technique has been used in the recent period but has not been explored with the sense of fabrication methodology. Mostly, biochar composite is used for adsorptive applications due to one of the most practical and cost-effective approaches commonly used for different environmental constraints (Grassi et al., 2012; Yang et al., 2019). Annually 1.3 billion tons of food waste is generated globally, which is equal to one-third of the global food production every year (Li et al., 2021). Among agro-food wastes, which primarily consist of fruit wastes, globally, around 637 million tons of fruit were produced in 2012. Almost, 75% of the world's citrus production comes from the USA, Brazil, China, Mexico, India, and Spain in which sweet oranges (*Citrus sinensis*) and mandarin oranges (*Citrus reticulata*) are the leading varieties of production from the citrus family, harvested primarily between December to March (Paggiola et al., 2016). Orange juice processing generates between 8-20 million tons of orange waste and more than 50% of this waste accounts for the orange peel (Aboagye et al., 2017). Elemental composition became an added advantage for particular usages, such as orange peel rich in hemicellulose, cellulose, lignin, and pectin, showing probable adsorptive application for different pollutants. Some of the studies have used orange peel as precursor feedstock for biochar due to its essential

ingredients (Liu & Zhang 2022). Composting of organic waste releases greenhouse gases, primarily methane which have more warming potential in comparison to CO2, and a large volume of eggshells are dumped at landfill sites (Zhang et al., 2022; Diaz et al., 2017; Scharff et al., 2009). Attraction towards waste biomass as a raw feedstock for biochar preparation was gained due to the growing concept of circular economy and the need for reducing more carbon footprint. Eggshells, due to their rich content of calcium carbonate, have been utilized as a natural source of calcium carbonate and have been used as a catalyst and adsorbent (Bakshi et al., 2016; Balakrishnan 2022; Diaz et al., 2017; Raheem et al., 2020; Chakraborty & alabro 2015; Dutta et al., 2018; Chakraborty et al., 2022; Phuong et al., 2017; Song et al., 2020).

1.1 Biochar

Biochar is a carbon rich solid product obtained by pyrolysis of biomass under no or oxygen-limited environments (Yi et al.2017). Biochar are mainly rich in functional groups, posses large surface area and high in mineral content, due to which their application has been used for different environmental constraints (Tan et al., 2015). The feedstock for biochar are generally from agricultural biomass, forest biomass and waste biomass such as straw, corn cob, animal manure ,wood chips, walnut shell , sewage sludge, pine cone and orange peel. The chemical composition of biomass primarily consists of cellulose, hemi-celluloses, lignin, organic extractives, and inorganic minerals.

The constituents percentage varies in different biomass species, due to high content of carbon and oxygen elements which facilitate the formation of various oxygenated functional groups such as (-COOH, -OH,-C-O-R) on the biochar surface. These groups serves as the active site for the different applications.The principle parameter which affect the physicochemical properties of biochar during preparation are pyrolysis temperature, heating rate and residence time (Ronsse et al., 2013). The effect of parameters are summarized in the table given below.

Table 1 Effects of pyrolysis temperature on the biochar physicochemical properties

Raw material	T(^{0}C)	Yield (%)	Ash (%)	BET (m^2/g)	V_{total} (cm^3/g)	pH	H/C	O/C	References
Orange peel	200	61.60	0.30	7.75	0.010	-	1.14	0.45	Chen and Chen (2009)
	300	37.20	1.57	32.30	0.031	-	0.78	-	
	400	30.00	2.10	34.00	0.010	-	0.58	0.22	
	500	26.90	4.27	42.40	0.020	-	0.38	0.21	
Rice straw	300	38.00	-	6.77	-	7.9	0.07	0.43	Shen et al., (2019)
	500	31.00	-	22.38	-	10.4	0.04	0.22	
	700	30.00	-	115.47	-	10.7	0.03	0.13	
Alfaalfa	350	47.70	7.10	3.50	-	-	0.80	0.20	Choi and Kan (2019)
	450	30.70	9.10	4.00	-	-	0.50	0.10	
	550	28.30	16.0	183.00	-	-	0.30	0.10	
	650	27.50	13.6	405.00	-	-	0.20	0.10	
Soybean stover	300	37.03	10.41	5.61	-	7.3	0.74	0.27	Ahmad et al., (2012)
	700	21.59	17.18	420.30	0.190	11.3	0.19	0.14	

Sewage sludge	500	63.10	74.21	25.42	0.056	8.8	0.09	0.45	Chen et al., 2014
	600	60.25	77.90	20.27	0.053	9.5	0.06	0.30	
	700	58.66	81.53	32.17	0.068	11.1	0.04	0.30	
	800	54.71	83.93	48.50	0.090	12.2	0.04	0.17	

Table 2 Effects of heating rate on the biochar physicochemical properties

Biomass	T (^{0}C)	Rate (^{0}C/ min)	Yield (%)	Ash (%)	BET (m^2/g)	V_{total} (cm^3/g)	pH	H/C	O/C	Reference
Wheat straw	450	2	-	3.90	178	0.184	-	0.40	0.40	Mohanty et al., (2013)
		450	-	3.60	184	0.179	-	0.60	0.40	
Pinewood	2		-	4.60	166.00	0.167		0.40	0.10	Mohanty et al., (2013)
	450		-	4.10	185.00	0.178		0.60	0.20	
Safflower seed cake	400	10	34.18	7.50	2.67	0.005	8.2	0.71	0.26	Angin.,(2013)
		30	30.00	8.40	2.26	0.004	7.6	0..6	0.27	
		50	29.70	8.50	1.89	0.004	8.1	0.64	0.26	
	500	10	28.90	8.50	4.23	0.080	9.4	0.5	0.23	
		30	27.80	8.60	3.98	0.075	9.5	0.49	0.25	

		50	26.00	8.70	3.64	0.069	9.3	0.48	0.23	
	600	10	26.20	9.20	3.41	0.006	9.9	0.38	0.20	
		30	25.30	9.30	2.85	0.005	10.2	0.38	0.21	
		50	24.40	9.50	2.47	0.005	9.8	0.43	0.21	

Table 3 Different preparation method of biochar from biomass

Feedstock	Temperature (°C)	Residence time (h)	Heating rate (°C/min)	Pyrolysis type	Pollutant	Reference
Rice husk	600	4.0	20	-	As(III), As(V) and Cd(III)	Wang et al., (2019a)
Orange peel	150-700	-	-	Slow pyrolysis	Naphthalene and I-naphthol	Chen and Chen (2009)
Cow dung	200, 350	4.0	-	Slow pyrolysis	Pb^{2+} and Atrazine	Cao et al. (2008)
Sludge	550	2.0	10	Slow pyrolysis	Pb^{2+}	Lu et al., (2011)
Oak	400, 450	-	-	Fast pyrolysis	Cd^{2+} and Pb^{2+}	Mohan et al., 2013
Municipal sludge	500-900	-	-	Fast pyrolysis	Cd^{2+}	Chen et al., (2014)
Pig manure	300-700	4.0	15	Slow pyrolysis	Cd^{2+}	Zhang et al., (2013)

Algae	203	2.0	-	HTC	-	Heilmann et al.,(2010)

1.2 Biochar composite

The pyrolysis technique is used to prepare the biochar composite, mostly biochar composites investigated are of biochar/metal oxide, and several studies are being reported in the context of wastewater treatment (Dong et al., 2019; Cheng et al., 2022). Mainly, for the synthesis of biochar-metal oxide composite, a metal impregnation process is applied (Wang et al., 2022; Liu et al., 2021; Zhang et al., 2021; Chen & Yuan 2022), in which a high volume of metal salt solution is prepared for soaking the biochar in it for the metal impregnation over its surface.

These processes for biochar composite create a secondary environmental risk (Premarathna et al., 2019a), and require several processing steps and resources as well. However, co-pyrolysis of orange peel with red mud has been studied, and their application was studied for heavy metal immobilization from wastewater (Cheng et al., 2022). Synthesis of biochar composite using co-pyrolysis of orange peel and chicken eggshell without any chemical modification has not been reported yet.

Table 4. Different Composites/Biochar listed with their source and modification

Composite/Biochar	Source	Modification	Reference
Biochar/Alginate	Corncob	$KOH/FeCl_3$	Liu et al.,2023
Silica-composited	Alkali-fused fly ash- Rice straw	NaOH	Wang et al., 2020
Zero-valent iron-lemon biochar	Lemon peel	$FeCl_3/NaBH_4$	El-Monaem et al., 2022
Geopolymer-biochar composite	Pozzolan-Sugarcane bagasse	Alkali activation	Dzoujo et al., 2022
Chitosan crosslinked composite	Corncob	Chitosan	Liu et al., 2022
Fe-sludge biochar composite	Bacillus sp.	Fe-sludge biochar	Ahmad et al.,2021
ZnO/biochar nanocomposite	Bamboo stakes	ZnO	Yu et al., 2021

1.3 Biochar activation

The activation route for the functional composites is primarily chemical-based, which results in the generation of secondary pollutants. The current activation route mainly uses metal impregnation and acid-base modification techniques for the modification (Heo et al., 2019; Jiang et al., 2019; Tang et al., 2022. In the past few years, biochar composites have been extensively investigated as a sorbent for different environmental remedial applications (Zhao et al., 2021; Safarik et al., 2016; Yu et al., 2022;). These functional composites require complex activation processes for higher effectiveness. The different routes for the activation

of these functional biochar composites involve physical, chemical, and biological modifications. Physical activation mainly involves steam, air, N_2, and CO_2, whereas chemical activation uses an acidic, alkaline and metal salt modification, whereas biological modification primarily incorporates an enzymatic mechanism(Rio et al. 2006; Mestre et al. 2007; Veksha et al. 2016 and Aworn et al. 2008; Singh et al. 2008; Toles et al. 2000; Cha et al. 2010; Tay et al. (2009); Nakagawa (2007; Tang et al., 2022). These activation routes involve complex processes with high-cost operating conditions and generate large volumes of waste and toxicity to the environment, which hinders practical application on a large scale (Schlagenhauf et al., 2015; Wang et al.,2021). At present, partial green synthesis utilizes the reduction of metal oxides from the biomass source and the zero-valent state of the metal for the application (Abdelfatah et al., 2021; Zhu et al., 2018; Chiou et al., 2013; Lorestani et al., 2015).

1.4 Biochar for Methylene blue

Biochar composite has been studied widely for wastewater treatment applications. Due to the rapid expansion of the textile industry, there is an increasing concentration of different dyes in wastewater, affecting human health and the water ecosystem synergistically (Ali., et al 2022; Ghaly et al. 2014). In recent years different biochar composites with modifications(mentioned in Table No. 3) have been applied for the sorption of Methylene blue, these modifications showed the complexity involved in the removal mechanism of Methylene blue. The composites prepared from the different wastes are mostly complex and alkali-modified to enhance cationic dye adsorption. The alkali modification provides the prime source of oxygenated-rich species as well as improves porosity. The unmodified

pristine biochar's main hindrance to their application are reduced active sites and porosity which leads to low adsorption capacity and quick saturation of the adsorbent.

The limited usage of chemically modified orange peel as a sorbent for Methylene blue has been reported in the literature(Kebaili et al., 2018), whereas, Amin et al. 2019 investigated the removal of methylene blue with the pristine orange peel biochar prepared at 800^0c, biochar prepared at high temperature are significantly deficit with functional group content. The literature suggested that most studies related to orange peel and other bio-composites for Methylene blue adsorption are confined to acid/base modification of the adsorbent. The limited studies need to be explored for the sorption of Methylene blue with a greater sustainability approach. The present study aims to optimize the novel combination of two bio-waste due to their rich elemental composition, for the synthesis of the functional composite.

Table 5. The chemical composition (dry basis) of Orange peel (Rivas et al., 2008)

Compound	**%**	**Compound**	**%**
Soluble sugar	16.90	Pectin	42.50
Starch	3.75	Ash	3.50
Cellulose	9.21	Fat	1.95
Hemi-cellulose	10.50	Protein	6.50
Lignin	0.84	Others	4.35

Furthermore, the proposed feedstock combination of orange peel and chicken eggshell has not been reported yet. The rich phenolic and flavonoid content of orange peel can add possible oxygenated groups and the alkaline nature of chicken eggshells can provide the best possible basic environment for precipitation. However, the literature lacks information regarding composite synthesis with the feasibility of two different wastes on the account for in-situ activation and using their application for Methylene blue removal.

A hypothesis was conceptualized to co-pyrolyze the orange peel and chicken eggshell together and optimize their synthesis parameters to see the effect of their chemical interaction and their effect on the natural fabrication of functional groups during the carbonization process. Preparatory parameters were optimized through the response surface optimization tool (RSM), this tool could also provide the ideal interaction proportionate between the orange peel and eggshell where natural fabrication can occur with the selected parameters, moreover, . The response surface methodology used the Box-Behnken Design tool for the experimental run to assess the effect of different input variable conditions on the response variable selected as the adsorption capacity for the methylene blue removal. The prepared composite was characterized to asses the given optimized condition effect over the composite surface enhancements such as porosity, functional groups, surface area, and crystallinity. The adsorption mechanism was well explained with the isotherm modeling. This objective promotes an integrative solution towards different environmental constraints, simultaneously, such as solid waste management, green activation sources, and water treatment.

1.5 Biochar for Bisphenol A

The biochar composite has been used for different organic, inorganic, and heavy metals but is less explored for emerging organic contaminants. Amongst the different emerging contaminants, the primarily emerging organic contaminant Bisphenol A (BPA) has been widely used in the plastic industry, which has raised serious concerns with its emerging concentration at different trophic levels. Bisphenol A (Ma et al., 2019; Schug et al., 2014; Hengstler et al., 2011) has also been classified as an endocrine-disrupting compound, which can interrupt the endocrine system by mimicking, blocking, or disrupting the functions of hormones in living organisms. Apart from this, BPA discharge from industrial and commercial sectors can affect different water ecosystems and can also lead to biomagnification of this respective compound (Wang et al., 2017; Torres-Garcia et al., 2022; Peng et al., 2018; Salgueiro-Gonzalez et al., 2015; Zhao et al., 2019).

The different methodologies adopted for the removal of BPA from the aqueous medium include advanced oxidation processes with persulfate/Fenton reagents, ultrasonic, microbial, adsorption, and biochemical technologies (Chu et al., 2017; Park et al., 2018; Diao et al., 2020). Among the discussed methodologies, adsorption is the most desired technique for easy operations with cost-effectiveness.

Table 6. Different Biochar composites for the removal of Bisphenol A

Biochar Composite	Feedstock	Activation source	Removal Mechanism	References
$CuZnFe_2O_4$	Bamboo	Metal oxide	Adsorption	Heo et al., 2019
Fe-Biochar	Saw dust	Fe Metal	Advance Oxidation Processes (AOP)	Jiang et al., 2019
Fe_3O_4-Biochar	Rice husk	Metal oxide	AOP	Cui et al., 2021
δ-MnO_2/KCF	Kenaf Bast Fiber	Metal oxide	AOP	Gan et al., 2021
H_3PO_4/Biochar	Corn straw	Acid modification	Adsorption	Zhao et al., 2017
$NaHCO_3$/ CO_2/Carbon composite	Shrimp shell@cellulose	Chemical/gas activation	Adsorption	Zafar et al., 2022
Biochar/iron oxide	Green algae	Metal oxide	AOP	Yu et al., 2022
CoP/N Carbon composite	Yeast extract	Metal oxide	AOP	Tong et al., 2020
Alkali modified Biochar	Wheat straw	NaOH	Adsorption	Tang et al.,2022
Fe_3O_4 Biochar	*Platanus orientalis* leaves	Fe_3O_4	AOP & Adsorption	Cui et al., 2021

The predominantly used methodology of advanced oxidation processes consumes a high amount of chemical reagents and secondary byproducts, making it not a wise option for long-term use (Anandan et al., 2020; Madima et al., 2020).

As per the current scenario of different emerging contaminants, especially BPA availability as pollutants (Kumar et al., 2022; Tang et al., 2020; Goeury et al., 2022), an environment-friendly approach that can be sustained for a long period and easy to operate needs to be

investigated with an urgent priority. The integrated approach for a complete green synthesis of the biochar composite and its application for BPA removal has not been studied yet, and few pristine biochars have been investigated as an adsorbent for BPA removal, but they are not very effective due to their low affinity and poor functionality. The research gap of absolute functionalized green sorbent and great affinity for BPA removal needs to be addressed, which can serve the current dual objectives.

In this study, a novel synthesis methodology has been developed to satisfy the dual objectives of complete green synthesis and great affinity for BPA molecules. This process approached with zero chemical synthesis, making it an absolutely green technique, moreover, with no toxicity effect of secondary byproduct. The in-situ activation technique was applied for the green modification by using chicken eggshell suspension as an activating source over orange peel biomass. The rich content of $CaCO_3$ in the eggshell made it a promising feedstock for natural activation (Kumar et al., 2024; Liu et al., 2019) sustainable source.

This approach facilitated the controlled oxidation of orange peel biomass and helped retain the cellulosic structure at high temperatures. The resulting orange peel composite (OPC9) characterization showed a high surface area with well-developed porosity, which showed the pores with a definite arrangement pattern, thereafter enhancing the pore diffusion property of the composite for modal pollutant BPA. This technique enhanced the mineral content of the composite, which provided an excellent affinity for chemisorption to contaminant molecules.

This methodology provided a novel route for maximizing the dual effect of chemisorption and physisorption with subsequent porosity and high mineral content for effective adsorption, which marked the developed technique as a proven methodology for no chemical synthesis formula. This approach could form the basis for the activation of different biomass-based adsorbents and widen their efficacy with increased affinity for different environmental constraints; furthermore, this will also lead to complete sustainability.

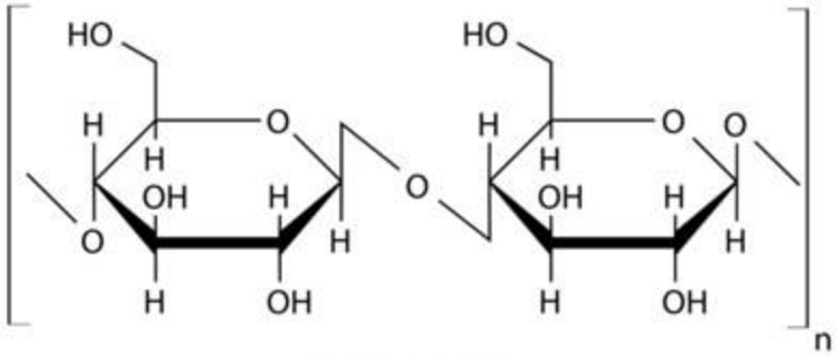

Cellulose

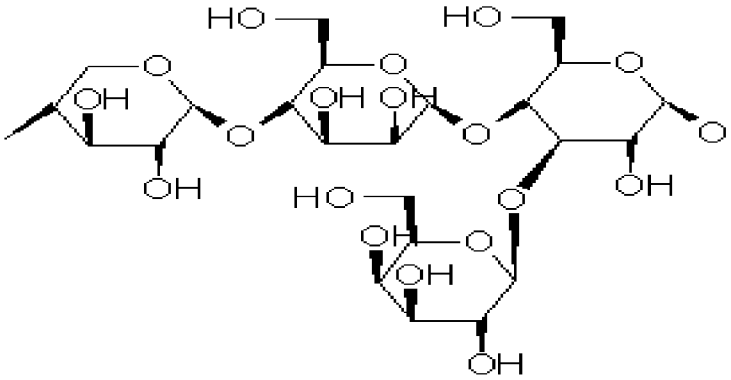

- Xylose - ß(1,4) - Mannose - ß(1,4) - Glucose -
- alpha(1,3) - Galactose

Hemicellulose

Lignin

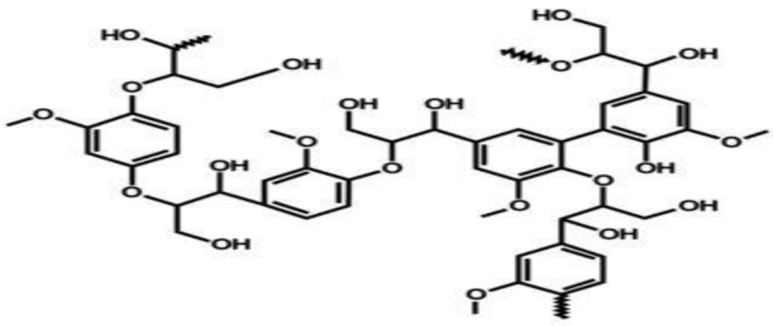

Fig 1. Images of the Cellulose, Hemicellulose and Lignin

1.6 The thesis structure

The chapter 1 describes the background regarding the biochar and different feedstocks, as well as the the feedstock selected for this work ,how much it accounts for the solid waste generation. The different activation route for composite synthesis, apart from this this section also discuss the different biochar composite state of the art for Methylene blue and Bisphenol A adsorption. The chapter 2 discuss the different physiocochemical properties of the biochar composite affecting the adsorption. Chapters 3 describes the methodology , which is divided into two parts as Methodology I &II. Both the methodology uses the same feedstock but different techniques for composite synthesis, methodology I used co-pyrolysis and optimized the pyrolyzing paramaters with RSM tool, where as, methodology II was a novel technique derived. The synthesised composite from methodologyu I was used for Methylene blue and from Methodology II it was used for Bisphenol A. The chapter 4 and 5 presents the results mainly from characterization and adsorption experiments, followed bt chapter 6 and 7 for conclusion and summary.

Part II

Biochar and organic contaminants interaction

CHAPTER 2

Biochar and organic contaminants interaction

2.0 Physicochemical properties of biochar affecting adsorption

2.1 Specific surface area

Higher, specific surface area provides active site for adsorption as well as inform about the degree of porosity (Ai et al., 2019; Kong et al., 2019). Although, the correlation between surface area and removal capacity cannot be estbalished linearly, as the adssorption performance of biochar for some pharmaceuticals compound such as diclofenac,acetaminophen, carbamazepine,citalopram and naphthalene enhanced with the increasing biochar's surface area (Solanki and Boyer, 2017; Zhang et al., 2019d). However,

effective adsorption has been shown by biochar with relatively low in surface area. Hence, the adsorption of organic contaminants by biochar depend on different conditions.

2.2 Surface functional groups

Biochar are relatively high in oxygenated groups such as hydroxyl and carboxyl groups (Kumar et al., 2024; Li et al., 2017b; Regkouzas and Diamadopoulos, 2019). These surface functional groups facilitate the interaction of H-bonding and π-π electron donor-acceptor (EDA) interactions (Mohan et al., 2014; Li et al., 2017 c; Pignatello et al., 2017). Furthermore, the hydroxyl groups acts as the electron donors and where as the carboxyl functional groups which has the receptive effects. Apart from this functional groups which contain phosphorus and sulfur could enhance the H- bonding interactions between the surface of carbonaceous adsorbent and aromatic hydrocarbons due to positive atoms (Tan et al., 2021). The oxygenated groups could increase the polarity,acidity and cation exchange capacity, which can eventually promote the adsorption of hydrophilic volatile organic compounds (VOCs) (Ahmad et al., 2014; Tan et al., 2015; Pignatello et al., 2017).

2.3 Pore size distribution

Pore size distribution can affect the adsorption of organic contaminants, the wide distribution of pore size , biochar with high porous structure can remove the organic contaminats with same molecular weight (Deng et al., 2017). The high energy adsorption sites available in the microporous structure could enhance the adsorption strength (Ersan et al. , 2017). The mesoporous range have been stated the best ideal range for organic contaminants due to possible increased pore size as well as the steric hindrance effect.

3.0 Effects of organic contaminants on adsorption

3.1 Hydrophobicity

The hydrophobicity plays crucial role in the adsorption of non polar organic pollutants. Biochar with low surface oxidation activity is hydrophobic and can remove organic pollutants with hydrophobic in nature with partioning adsorption mechanisms (Inyang and Dickenson, 2015; Zhang et al., 2019d). Adsorption of hydrophobic organic contaminants is a surface phenomenon, biochar with high aromaticity favours more hydrophobicity. The hydrophobic organic compounds driving force for adsorption mainly includes pore-filling and π-π interactions.

3.2 Molecular structure and weight

The physicochemical properties of organic contaminants, including molecular structure and molecular weight can significantly affect the adsorption process(Ahmad and Hameed, 2018; Solanki and Boyer, 2019d; Zhang et al., 2019d). Moleculae weight could produce an effect which can make pollutant diffuse in to adsorbent pores with a diameter bigger than its kinetic diameter.

3.3 Aromaticity

Aromaticity could affect the π-π elcetron donor acceptor interactions between biochar and adsorbates(Dai et al., 2019). The biochar produced at high pyrolysis temperature are rich in aromatic groups. These groups can attaract the pollutants with poly aromatic hydrocarbons.

3.4 Substituent groups

The substituent group of organic contaminants can enhanced the cation exchange capacity and can form the surface complexation with biochar(Mandal et al., 2017). The oxygenated rich biochar can easily form hydrogen bonding with pollutant with H ligand or an H acceptor group to reinforce adsorption. Different functional groups of pollutants such methylene blue ,tetracycline and herbicides which could be used as H- donor or H- receptor (Wang et al., 2015a; Fan et al., 2017; Karunanayake et al.,2017; Zhou et al., 2019).

3.5 Polarity

The organic contaminants aromatic rings interact with adsorbent aromatic rings for polar attractions .The increased polarizability of compounds caused the enhancement of π-π EDA interactions (Zhou et al., 2019). The most specific π-π interactions are occurred between oppositely polarized aromatics and weak occurs between same polarized aromatics.

Table 7

Adsorption mechanism for different organic contaminants in water with biochar.

Compounds	Contaminants	Feedstock	Pyrolysis temperature	Mechanisms	References
Pesticides	Carbaryl and atrazine	Pig manure	350 and 700^{o}C	Hydrophobic effect,pore filling and π-π EDA interactions	Zhang et al., (2013a)
	Boscalid	Rice straw	450^{o}C	π-π dispersive interactions, van der Waals forces & H-bonding	Taha et al., (2014)
	Norflurazon	Grass &wood	200-600^{o}C	London forces & π-π EDA interactions	Sun et al.,(2011)
	Paraquat	Swine manure	400^{o}C	Ion exchange	Tsai and Chen(2013)

	Pentachlorophenol	Reed	300-600^{o}C	π-π EDA interactions & Hydrophobic interaction	Peng et al.,(2016)
	Chlorfenvinphos	Corn stover	450^{o}C	π-π dispersive interactions, van der Waals forces & H-bonding	Taha et al., (2014)

Part III

Objectives of the thesis

CHAPTER 3

Objectives of the thesis

Following are the objectives of the thesis:

- Develop a green fabrication methodology for biochar composite synthesis.
- Selection of the optimal feedstock for the composite synthesis on the basis
- of elemental composition.
- Assessment of the physicochemical properties of the synthesized composite.
- Application of the composites for the adsorption of Bisphenol A and Methylene blue.
- Underlying the adsorption mechanism and affinity for modal organic pollutants.
- Studying the isotherm and kinetic modeling for visualizing adsorption behavior.

Part IV

Methodology

CHAPTER 4

Methodology

4.0Methodology -I EOC300 Composite

4.1 Chemical reagents

All chemical reagents, including (methylene blue) are of analytical grade and were purchased from VWR Chemicals.

4.2 Preparation of the eggshell orange peel biochar composite(EOC300)

Orange peel was collected from a local juice shop and initially washed with tap water, later with deionized water to remove the surface impurities. Afterward, it was oven dried at 100^0C for 24 h or until constant weight, then after it was ground and sieved to a particle size range of 100 µm- 500 µm. The waste chicken eggshell was collected from a local fast food shop and processed with similar conditions as orange peel. Subsequently, three different mass ratios (MR) of orange peel were taken and mixed with a fixed weight of the eggshell powder suspension, the suspension was stirred overnight at room temperature (± 25^0C), and then the resultant suspension was oven-dried at 100 ^{0}C for 24 h. The obtained material was pyrolyzed in the tubular furnace under an N_2 atmosphere with a flow rate of 10 cm^3/g. Finally, the received carbonized composite was washed with deionized water to remove the surface impurities, oven-dried at 110^0C, and kept in the air-sealed container for further use.

4.3 Design of experiment

The RSM is a multivariate statistical analysis tool, providing the advantage of using individual parameters and their interaction simultaneously. In the response surface methodology response variable is represented as "y," and different input variables for optimization are depicted as x_i (i=1, 2, 3….k). The relationship between the response variable and input variables is established by the second-order polynomial equation given by equation (1).

$$Y = \beta_0 + \sum_{i=1}^{k} \beta_i x_i + \Sigma_{i=1}^{k} \sum_{j=1}^{k} \beta_{ij} x_i x_j + \sum_{i=1}^{k} \beta_{ii} x_i^2 \quad (1)$$

where y is the response projected; x_i and x_j are the input variables, whereas β_0, β_i, β_{ij}, and β_{ii} are the regression coefficients for intercept, linear effect, quadratic effect, and interaction effect, respectively.

Validation of the polynomial model is tested using Analysis of variance (ANOVA) to analyze the significance of input parameters. The Minitab trial version application software was used to design the experiment and for data analysis.

In this study, the adsorption capacity was used as the response variable, and pyrolyzed temperature, the mixing ratio of eggshell to orange peel, and residence time as the independent input variables to prepare the composite. A series of 17 experiments were designed using Box-Behnken design from RSM to obtain the experimental data, and the number of experiments was calculated using equation (2), and the experiment was conducted with a prepared stock of 50 mg/l of methylene blue solutions.

$$N = 2k\,(k-1) + C_0 \qquad (2)$$

Where k is the number of input variables, and C_0 is the number of central points. The input variables with their selected range with low, high, and middle levels of each variable are designated as -1, +1, and 0. These above-discussed parameters with their range are summarized in the below matrix.

Table 8

Parameters matrix with their levels

S.No	Independent Variable	Unit	Code	Levels		
				-1	**0**	**+1**
1.	Temperature	^{0}C	X_1	300	500	700
2.	Mix ratio (MR)	g/g	X_2	1:1	1:2	1:3
3.	Residence time	hr	X_3	1	1.5	2.0

4.4 Batch sorption study

Sorption kinetics of methylene blue over orange peel biochar composite was performed with the batch experiments. Experiments were conducted in the Erlenmeyer flasks containing 50mL of methylene blue solution and eggshell orange peel composite(EO composite); 0.05 g of EO composite was stirred in a 250 mL Erlenmeyer flask containing 50mL of methylene blue solution until obtaining the adsorption equilibrium. The residual concentrations were analyzed with a UV spectrophotometer with χ_{max} at 665 nm. Adsorption capacity and removal efficiency were calculated with the following equations:

$$Q_e(mg|g) = \frac{C_0 - C_e}{w} * V \quad (3)$$

$$\text{Removal } (\%) = \frac{C_0 - C_e}{C_0} * 100 \quad (4)$$

where C_0 and C_e are the initial and equilibrium methylene blue concentrations(ppm), v (mL) is the volume of methylene blue solution, and w (g) is the weight of the adsorbent.

5.0 Methodology -II OP9 & OPC9

5.1 No chemical requirements

No chemicals were used for the composite synthesis, complete 100% green synthesis.

5.2 Synthesis of pristine orange peel biochar (OP9)

The orange peel was collected from a local juice shop, washed several times with distilled water to remove the surface impurities, and oven-dried at 100 ^{0}C until constant weight. Then after, it was processed to fine powder, with the help of an electric grinder, and later sieved the powder in a particle size of 100 µm- 500 µm. The processed orange peel powder was carbonized using a slow pyrolysis technique at 900 ^{0}C for 30 minutes with a heating rate of 2 ^{0}C/min in the tubular furnace under an N_2 atmosphere. After cooling down the furnace, the pyrolyzed material was taken out and washed repeatedly with deionized water until the material had a constant pH. After that, the material was oven-dried at 100 ^{0}C overnight and kept in an air-tight vial for further use.

5.3 Synthesis of orange peel composite (OPC9)

The primary raw materials utilized for the composite synthesis were waste orange peel and used chicken eggshells, which were collected from a local bakery shop, washed several times with deionized water to remove the surface impurities, and processed into a fine powder of particle size between 100um-500um and stored in an air-tight container for further use. Synthesis of the composite involved three simple steps. Firstly, the eggshell was prepared in distilled water by mixing 2 gm of eggshell powder in 100 mL of distilled water, and the suspension was stirred for one hour at 60^{0}C. The suspension was filtered and later on and mixed with 20gm of processed orange peel powder. The mixture was heated in a water bath

overnight at 60^0C. The impregnated mixture was oven-dried at 60^0C for 8-10 h, and slow pyrolysis was performed in the tubular furnace at 900^0C with a heating rate of 2^0C/min for 30 minutes under an N_2 atmosphere. The finally obtained Carbonized material was washed repeatedly with distilled water to remove the impurities and to achieve a constant pH. Thereafter, the received material was oven-dried for 24 hrs. and kept in the air-tight bottle for further use.

5.4 Characterization

The surface crystalline structure of the composite was characterized by powder X-ray diffraction (XRD) using a diffractometer with Cu K_α radiation (λ = 1.5406 Å) at 40 kV and 30 mA over 2ɵ range from 10^0 to 90^0. The morphologies and elemental mapping of the composite surface were investigated by scanning electron microscope coupled-energy dispersive spectroscopy (SEM-EDS). The specific surface area was measured using nitrogen adsorption/desorption isotherms at -195.8 ^{0}C by Micromeritics automated specific surface area and porosity analyzer. The specific surface area (S_{BET}) was calculated using the Brunauer-Emmett-Teller (BET) method, and porous characteristics were analyzed as per the Barrett-Joyner-Halenda (BJH) model. The surface functional groups were examined using the Fourier transform infrared spectroscopy(FT-IR) in the range from 400-4000cm^{-1}.

5.5. Bisphenol A (BPA) adsorption experiments

Adsorption isotherm and kinetics of BPA removal were studied with batch sorption experiments to assess the pristine orange peel biochar and orange peel composite as an effective sorbent for BPA removal. The isotherm studies were obtained by adding 0.05g of sorbent in a 100 ml Erlenmeyer flask with different initial concentrations (5-100mg/l) of BPA solution. The samples were agitated for 24 h on an orbital shaker at a room temperature of 25^0C ± 0.5 ^{0}C, then the solutions were filtered through a 0.45µm pore size nylon membrane filter, and residual concentration was measured. Sorption kinetics were performed with a 50mg/l concentration of BPA in a 100 mL Erlenmeyer flask by mixing 0.05g of sorbent in a 50 ml solution of BPA. The samples were shaken at a room temperature of 25^0C and were taken out for measurements at intervals of 5,30,60,90,120,240 and 360 minutes. The experimental data were fitted with the linear kinetic model of pseudo-first order and pseudo-second order, and equations are expressed below in Eqs. (5) & (6). The analysis was performed with a UV- spectrophotometer at a wavelength of 272 nm for BPA residual concentration measurement.

Pseudo-first order: $$\log(Q_e - Q_t) = \log Q_e - \left(\frac{k_1}{2.303}\right) t \quad (5)$$

Pseudo-second order: $$\frac{t}{Q_t} = \frac{1}{k_2 Q_e^2} + \frac{t}{Q_e} \quad (6)$$

where Q_e and Q_t (mg/g) are the adsorption capacity of the adsorbents at equilibrium and at a given time, k_1 (h^{-1}) and k_2($g.mg^{-1}.min^{-1}$) are the adsorption rate constants of the kinetic

models, respectively. The amount of BPA adsorbed on the adsorbent at equilibrium (Qe) and adsorption capacity can be calculated with the equation mentioned below.

$$Q_e = \frac{(c_0 - c_e) \times v}{m} \quad (7)$$

Where C_0 and C_e (mg/l) are the concentration of BPA at the initial and equilibrium, respectively, v is the volume of BPA solution, and m (g) is the mass of the adsorbent used.

5.6 Effect of initial pH

The effect of the initial pH of the working solution for BPA adsorption was studied, where the initial pH of the solution was adjusted with 0.1 M HCl or NaOH to 3,4,5,6,7,8,9,10 and 11 respectively, thereafter 0.05 g of adsorbents (OP9 and OPC9) separately stirred in the water bath at room temperature 25 ^{0}C for 24 h, then after supernatant was measured for BPA concentration.

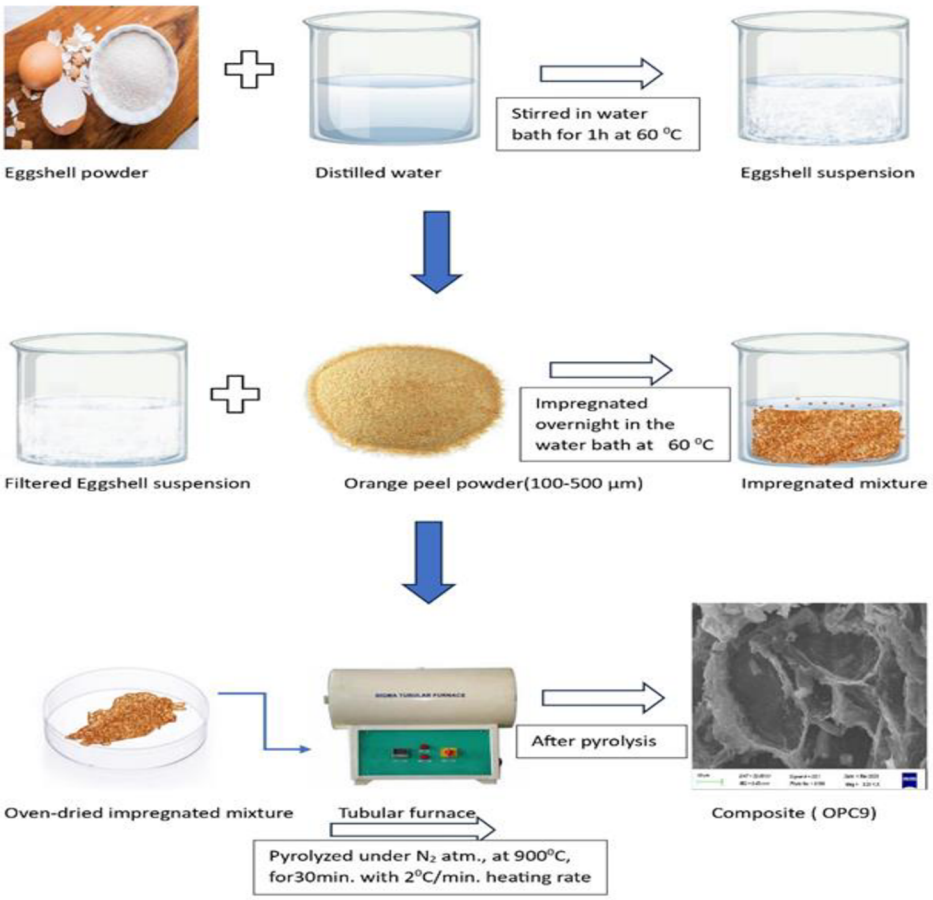

Fig 1: Schematic representation of Composite synthesis (OPC9)

Fig.2 Schematic representation of Composite synthesis (OPC9)

PART V

RESULTS & DISCUSSION

CHAPTER 5

Results and Discussion

6. Characterization

6.1 EOC300 &OP300 composite

6.1.1SEM-EDX analysis

The scanning electron microscope (SEM) images of the orange peel composite are shown in Figure 3(a). The SEM image of the composite showed a smoother surface and displayed lots of fragments with rich defect structure and porosity, these defects were favored by the release of volatile components and the possible acetate group formation, due to different elemental compositions giving their suspension an alkaline and a slightly acidic pH, opened possibilities for acetate formation, which added the more porous site to the composite surface, treatment of orange peel biomass with eggshell suspension provided stable and controlled oxidation which, facilitated the small defect structures and enhanced pore volume supported by N2 adsorption isotherm. Post-sorption SEM analysis in Figure below showed the adsorbed methylene blue over the porous surface which was supported by the EDS analysis, post-sorption images clearly showed the pore-filling mechanism as well as a great extent of physisorption. EDS analysis of the composite confirms the higher oxygen atomic percentage, indicating the rich oxygen group over the composite surface. The Co-pyrolysis

technique, with this novel combination enhanced calcium content, which improved surface complexation process for more effective adsorption. While Post-sorption EDS analysis confirms the higher atomic percentage of atomic carbon for effective interaction between composite and the methylene blue.

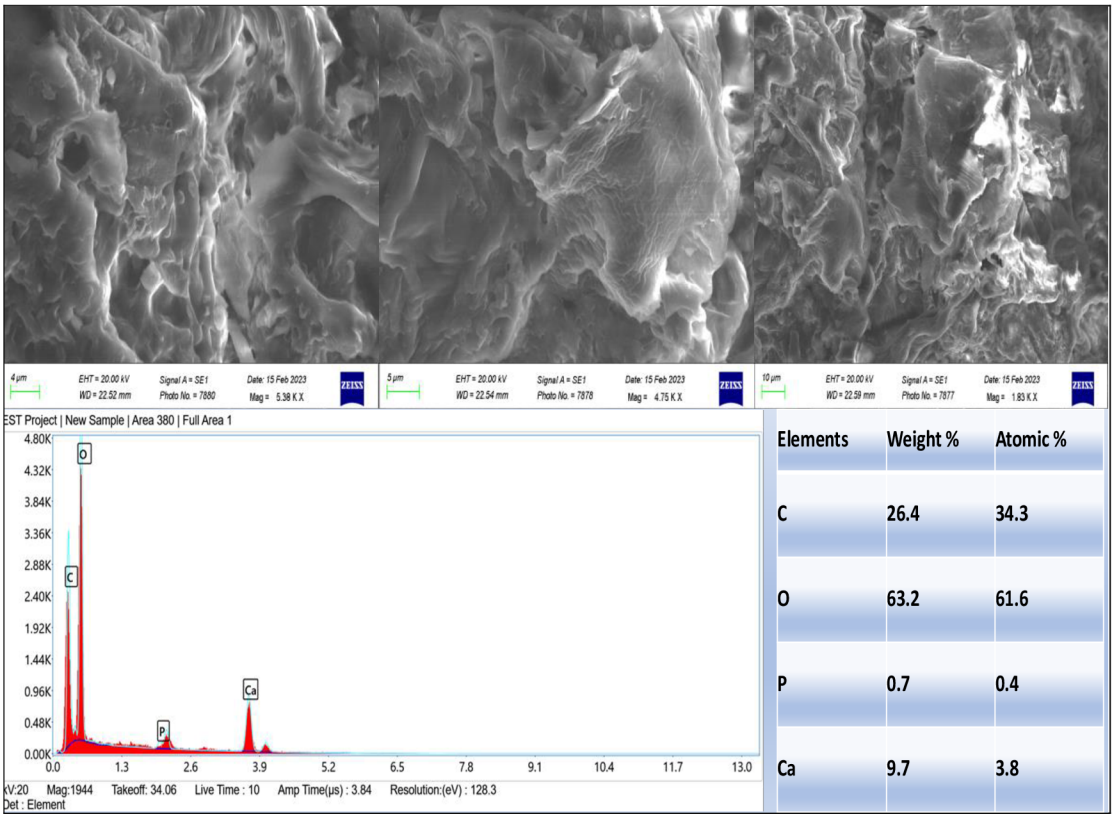

Figure 3. (a)SEM-EDX Aanalysis of EOC300

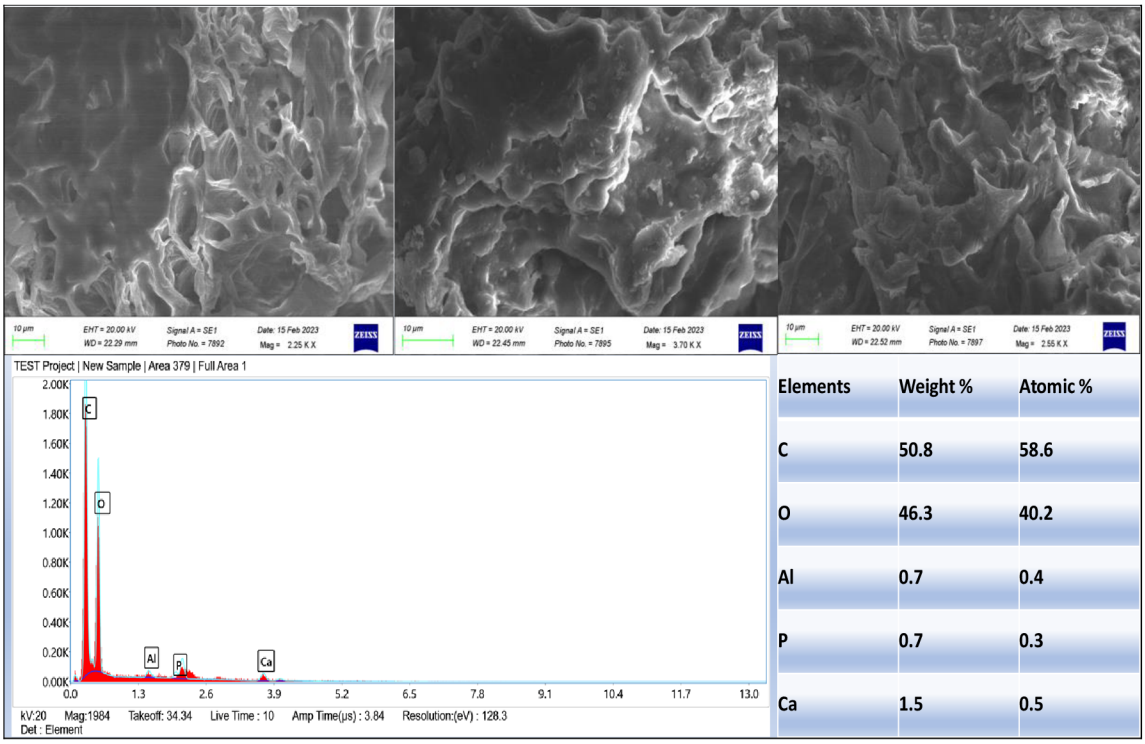

Elements	Weight %	Atomic %
C	50.8	58.6
O	46.3	40.2
Al	0.7	0.4
P	0.7	0.3
Ca	1.5	0.5

Figure 4(b) SEM-EDX Aanalysis - Post sorption(Methylene blue) EOC300

6.1.2 XRD analysis

The XRD(X-ray diffraction spectroscopy) pattern of the biochar composite shows the non-crystalline amorphous phase, and the intensity of peaks are sharp and flattened broadness of the composite with respect to the orange peel biochar pattern. XRD characterization indicated the successful composite formation with intense peak Q, confirming the suspension of orange peel and eggshell interacted with each other and the presence of $CaCO_3$, KCl, and MgO also confirms the uniformity of the composite. Composite's surface crystallinity and the corresponding peaks. It can be seen in Figure 3 that the XRD patterns of the composite showed a better amorphous phase with major peaks at 30^o,50^o corresponding to the characteristic crystal planes of inorganic components $CaCO_3$.

6.1.3. FTIR analysis

FTIR characterization determines the vibrational frequency of the functional group present on the surface of the compound, prepared composite (EOC 300) surface molecular structure was investigated by Fourier Transform Infrared Spectroscopy (FTIR), eggshell-orange peel composite (Fig. 2.), shows the major broad molecular stretch from 1150 cm^{-1} to1650 cm^{-1} ascribed to the molecular stretch of COOH (OH bending) group, narrow band at 850 cm^{-1}(C-H) and 3500cm-1(OH), spectra showing between 3200-3500 cm^{-1} showing the dehydration of cellulosic and ligneous components begin at 300 °C, whereas there was no significant difference between the orange peel biochar, co-pyrolysis of eggshell with orange peel enhanced the functionality of the composite as the functional peak showed in the eggshell FTIR spectrum**,** with respect to carbonized orange peel, which was stated by the peak broadness and their intensity at 1408 cm-1 showed the strong presence of O=C=O group, whereas molecular stretch at 3500 cm-1 attributing the intermolecular bonded OH- group, moreover, peak as 1565 cm-1 showing the C=O group. A small peak at 862 cm^{-1} identifies the C-H group, peak at 1043 cm^{-1} corresponds to the symmetric stretching vibration of the C-O group. FTIR, characterization confirms the successful attempt of co-pyrolysis to fabricate the oxygenated functional group over the composite surface.

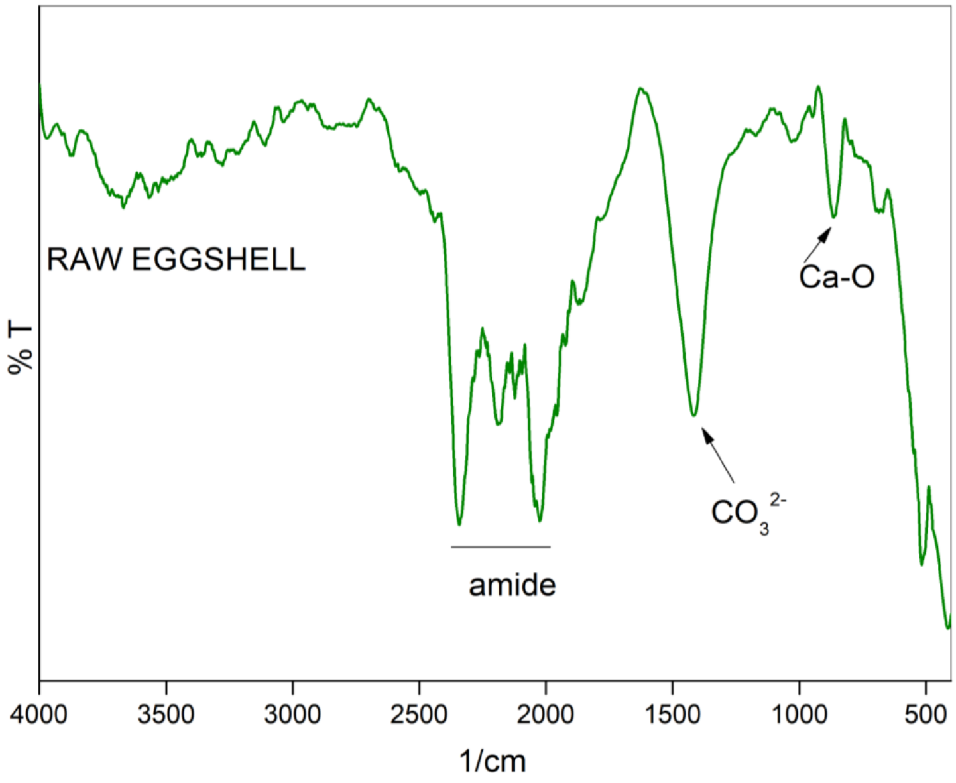

Figure 5. FTIR image of Raw Chicken Eggshell

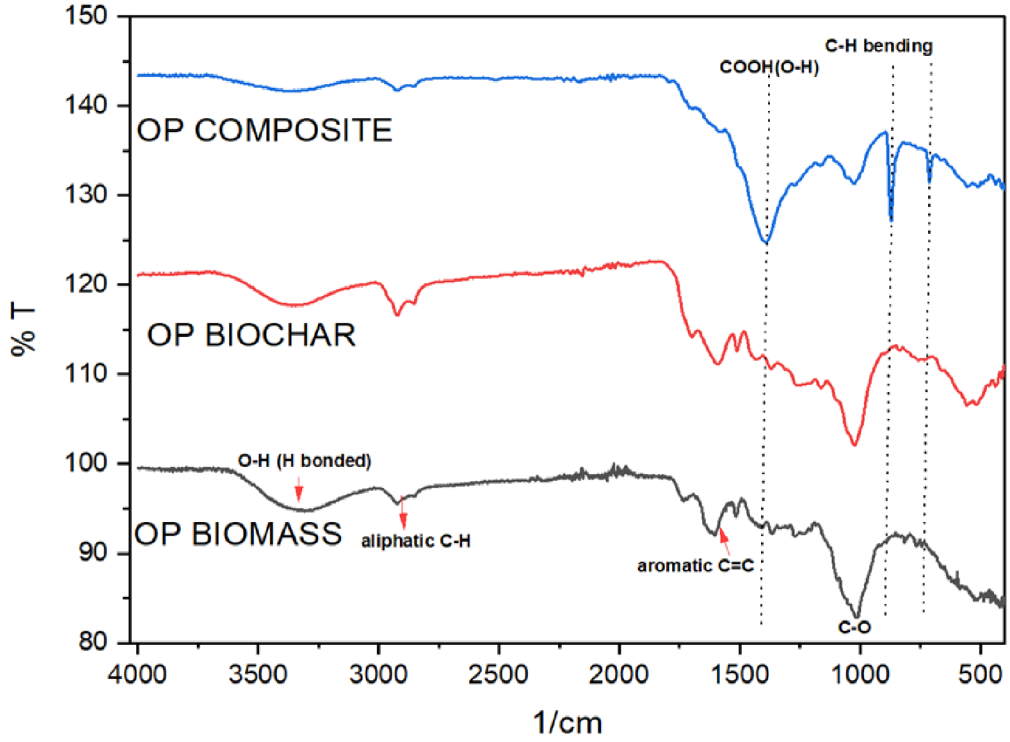

Figure 6. FTIR images of Orange peel biomass, OP300 & EOC 300(OP Composite)

6.1.4 BET analysis

The measured surface area of the carbonized orange peel was $1m^{2,}$ whereas the composite was $64m^2$ with an average pore diameter size of 0.8nm with a more microporous structure of the composite. The composite showed around 60 times higher than the unmodified pyrolyzed orange peel. The adsorption isotherm resembles the type I pattern. This increased surface area may be explained by the presence of an enhanced functional group over the composite surface. This can be supported as well with the FTIR additional peaks. Adsorption/desorption isotherm and pore size distribution are shown in Figure3.

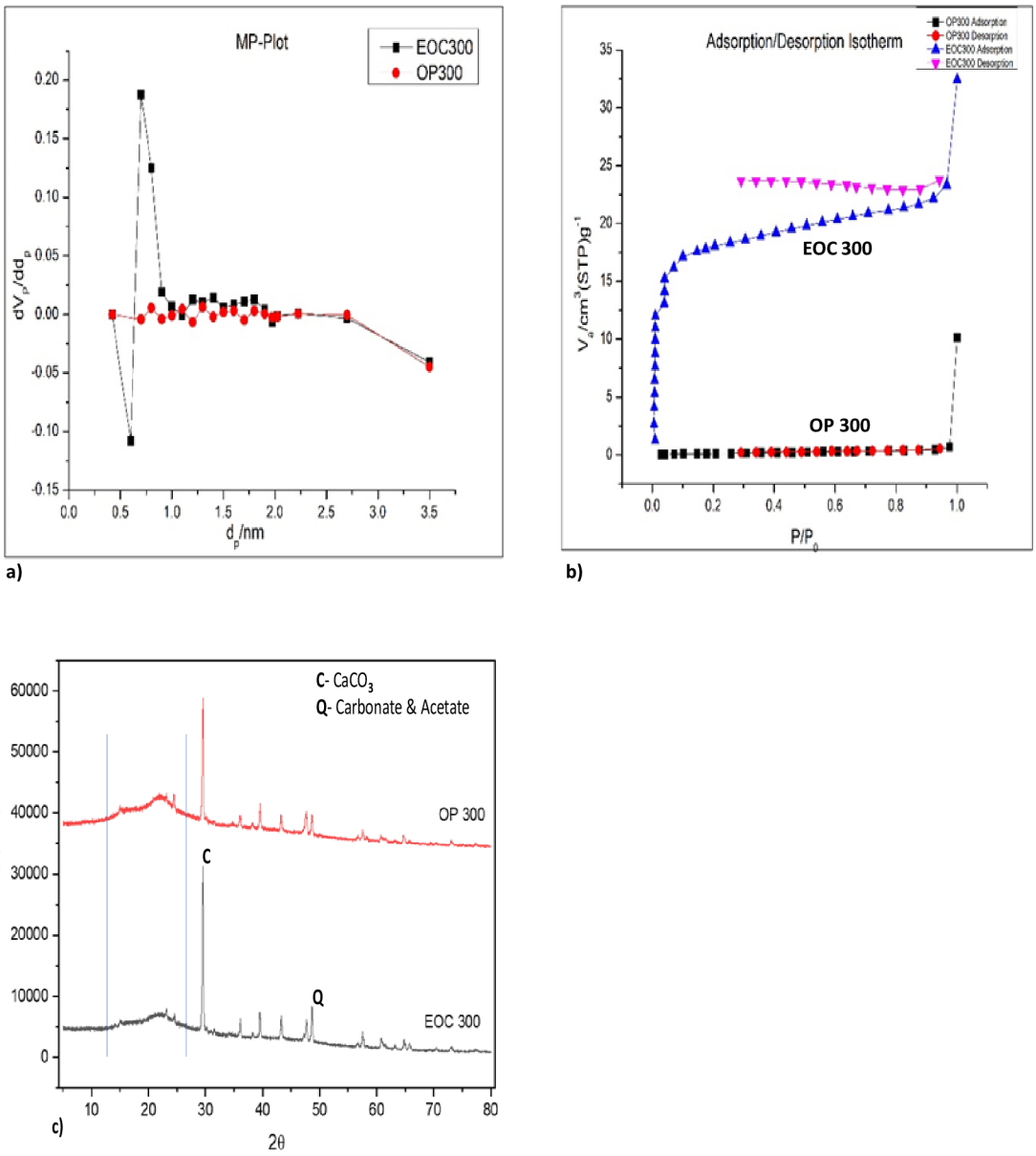

Figure 7.a) MP-Plot, b) Adsorption/ Desorption isotherm, c) XRD spectrum for OP300 &EOC300

6.2 Experimental results

EOC300 & OP300 Composite

The experimental results were obtained with the randomized experiments conducted as per the BBD-designed experimental sequence mentioned in presented Table. The empirical model was fitted with response variable data using regression analysis. The experimental matrix provided by the BBD and their respective responses is presented in respective Table. Statistical significance and regression equation evaluated using Minitab 19 software trial version. The developed model with the experimental values of adsorption capacity is given in Eqs.8

Regression equation in the coded unit

$$Y1=97.2-0.1905X1+39.2X2-43.4X3+0.000134X1^2-9.24X2^2+10.67X3^2-0.0203X1*X2+0.0257X1*X3-8.57X2*X3 \quad (8)$$

Where X1, X2, and X3 represent the three input variables, i.e., pyrolysis temperature, mixing ratio, and residence time, respectively. Analysis of variance (ANOVA) was applied to evaluate the goodness of fit.

6.2.1 Analysis of variance (ANOVA)

As per ANOVA analysis, the temperature parameter, amongst other variables, shows the highest effect on the adsorption capacity, with an F- value of 66.93. X1, $X1^2$, X3, and $X3^2$ are remarkable model terms for the effective chemical property. Amongst the selected input variables, the mix ratio of orange peel to eggshell was best optimized with equal proportions, which provided improved adsorption capacity, equal proportion led to the successful interaction for possible acetate intermediate and fabrication of calcium ions to the feedstock biomass. The residence time of pyrolysis when increased between one hour to two hours, induced wider thermal cracks, leading to the opening of wide pores and less pore volume, with reduced adsorption capacity. The 3D surface plot shows the interaction effect of selected parameters, initial temperature (300^0C), and residence time(1h), which contributed to the highest adsorption capacity; the interaction plot between them shows a negative relation with increasing temperature and residence time for adsorption capacity. Similarly, the same effect was observed with temperature and mixing ratio interaction.

Table 9

Results of the Box–Behnken design.

Run	Independent variables				Experimental value	Predicted value
	Blk	X1	X2	X3	Y1	Y
1	1	300	1:1	1.5	31.77	33.59
2	1	700	1:2	2.0	20.42	22.56
3	1	700	1:2	1.0	20.45	21.53
4	1	300	1:2	1.0	41.71	39.13
5	1	500	1:2	1.5	20.45	20.25
6	1	500	1:1	1.0	26.47	26.81
7	1	500	1:2	1:5	20.45	20.25
8	1	700	1:3	1.5	20.45	18.21
9	1	500	1:2	1.5	20.45	20.25
10	1	500	1:2	1.5	20.45	20.25
11	1	500	1:1	2.0	20.54	19.70
12	1	300	1:2	2.0	31.39	29.88
13	1	300	1:3	1.5	26.10	27.82
14	1	500	1:2	1.5	20.45	20.25
15	1	700	1:1	1.5	20.45	18.29
16	1	500	1:3	1.0	20.43	20.88
17	1	500	1:3	2.0	20.50	

X1 = Co-pyrolysis temperature, X2= Mixing ratio, X3 = Residence time, Y1 = Adsorption capacity.

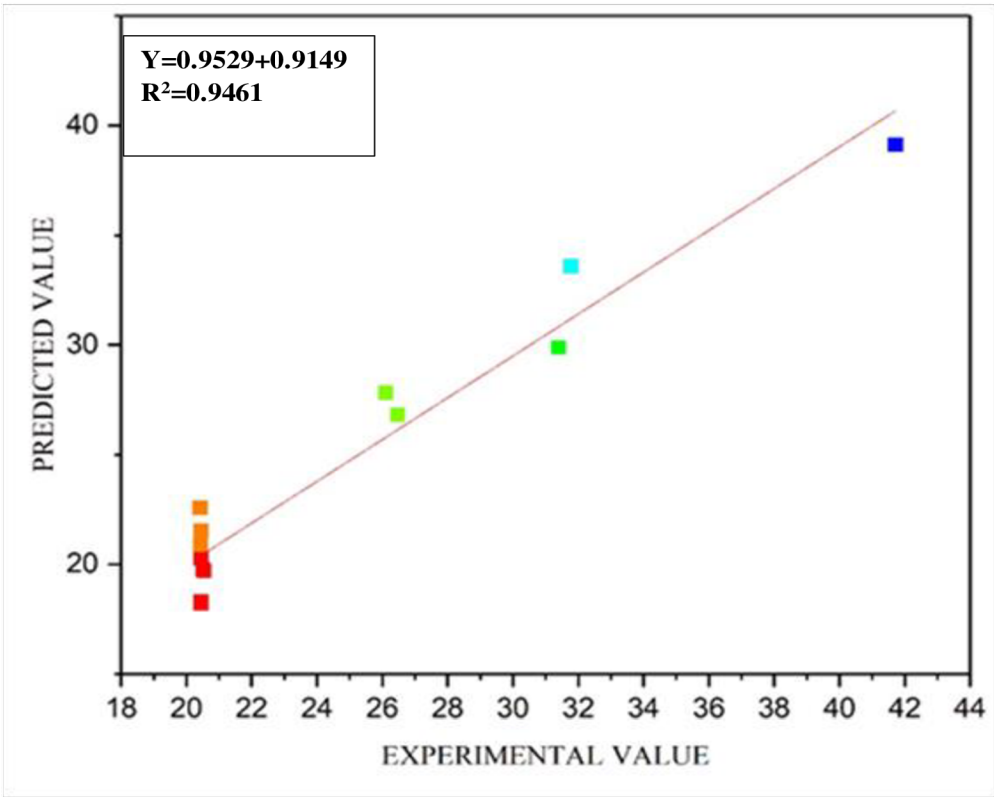

Figure 8 Correlation plot between Experimental value and Predicted value

Table 10

ANOVA for the regression model and respective model term for adsorption capacity (Y1)

Response	Source	Sum of Squares	Degree of freedom	Mean square	F- value	Prob > F
Adsorption capacity (mg/g)	Model	556.312	9	61.812	13.68	<0.001
	Linear	352.538	3	117.513	26.01	<0.000
	(Temp.) X1	302.399	1	302.399	66.93	<0.000
	(Mix Ratio) X2	17.273	1	17.273	3.82	0.091
	(Res.Time) X3	32.866	1	32.866	7.27	<0.031
	$(X1)^2$	121.565	1	121.565	26.91	<0.000
	$(X2)^2$	5.432	1	5.432	1.20	<0.309
	$(X3)^2$	29.891	1	29.891	6.62	<0.037
	X1*X2	8.043	1	8.043	1.78	0.224
	X1*X3	26.465	1	26.465	5.86	0.046
	X2*X3	9.014	1	9.014	2.00	0.201
	Residuals	31.627	7	4.518	-	-
	Lack of fit	3	31.627	10.542	-	-
	Pure error	4	0.000	0.000	-	-

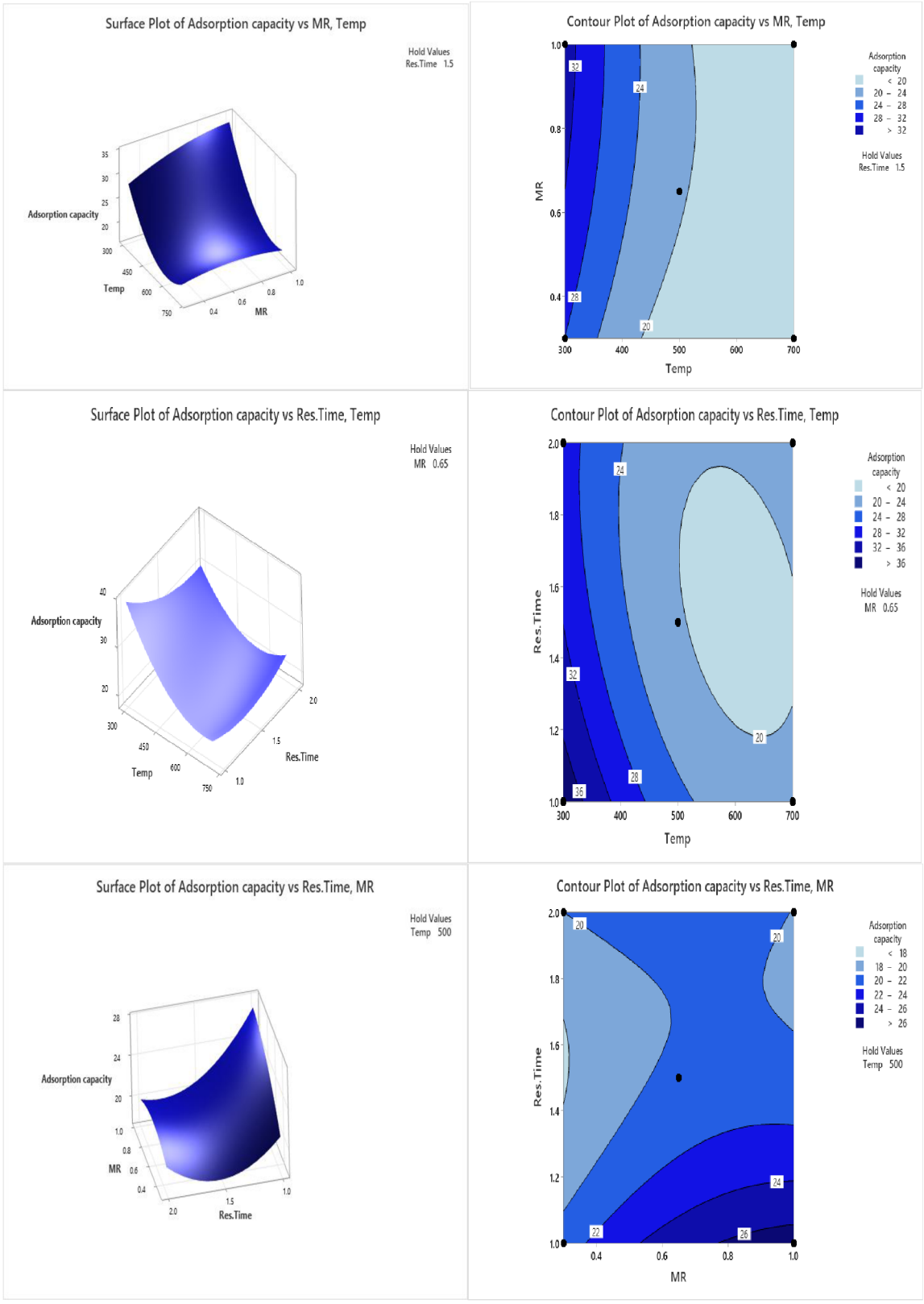

Fig.9(a-c) Shows the 3D surface plot and fig.(d-f) shows the contour plot for adsorption capacity with selected preparatory inputs.

Figure 5(a to f) shows the surface and contour plot showing the effects of different input co-pyrolysis parameters over the output parameter i.e. the adsorption capacity, figure 5 (c), clearly shows the dual interaction of input variables with adsorption capacity. The dark shade represents the region of effective adsorption capacity. The surface plot shown in the (fig. 10 (a)) illustrated the positive relationship with the mixing ratio and the negative relationship with co-pyrolysis temperature and residence time over adsorption capacity.

6.2.2 Adsorption mechanisms

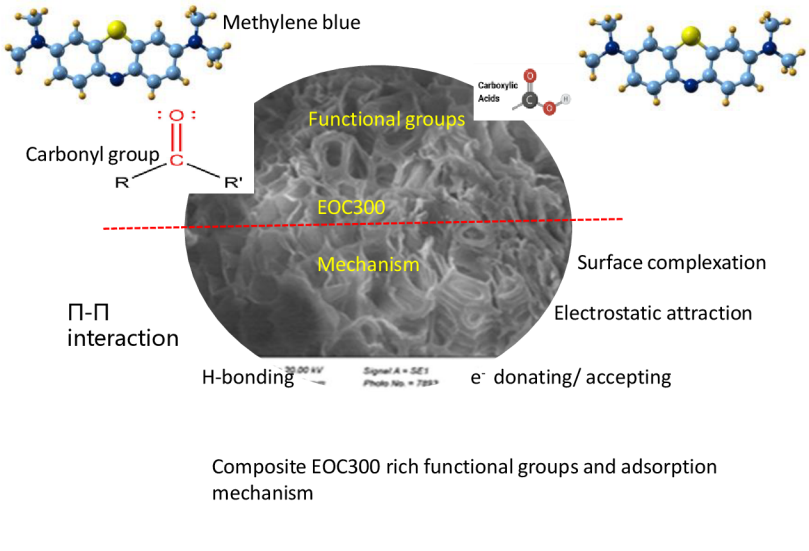

Composite EOC300 rich functional groups and adsorption mechanism

Fig.10 EOC300 Functional groups and adsorption mechanisms.

The adsorption mechanism of methylene blue removal on the composite was studied with the help of the isotherm model. Enhanced adsorption behavior of the composite can be explained by the increased surface oxygenated functional groups which increased the different adsorption mechanisms associated with it. A stock solution with a concentration of 100 mg L^{-1} of methylene blue was prepared, and by diluting the stock solution, the desired concentrations were prepared.

Batch sorption experiments were performed in Erlenmeyer flasks at room temperature ±25°C at 300 rpm. An adsorption isotherm study was performed by varying the initial methylene blue concentrations such as 10,20,30,40,50,60,70,80,90,100 ppm, and the suspension was stirred for a respective time. It was filtered with a 0.25 µm nylon membrane filter, and the residual concentration was measured using an ultraviolet spectrophotometer at 665 nm.

Freundlich and Langmuir's isotherms were applied to fit the experimental data. The Langmuir model defines the monolayer adsorption over a homogeneous surface with a finite number of adsorption sites with no or little interactions between the adsorbate and adsorbent.

6.2.3 Adsorption isotherm modeling

Expression for the linear form of Langmuir equation:

$$1/q_e = 1/q_m K_L C_e + 1/q_m \quad (9)$$

Where C_e (mg/L) and q_e (mg/g) are the equilibrium concentration and adsorption capacity, q_m (mg/g) and K_L(L/mg) are the maximum adsorption capacity and Langmuir constant, respectively.

Freundlich isotherm model states that adsorption occurs on the heterogeneous surface over different sites with different adsorption energies and confirms the interaction between the adsorbed molecules.

Expression for the linear form of the Freundlich equation:

$$\text{Log } q_e = \log K_F + 1/n \log C_e \quad (10)$$

Where 1/n and K_F [(mg/g). $(L/mg)^{1/n}$] are the Freundlich constants for adsorption feasibility and the adsorption capacity of the adsorbent.

Table 11

EOC 300 Langmuir and Freundlich constants for methylene blue adsorption.

Langmuir isotherm coefficient			Freundlich isotherm coefficient		
q_m (mg/g)	K_L (L/mg)	R^2	K_F[(mg/g). (L/mg)$^{1/n}$]	1/n	R^2
167.50	0.0616	0.94	10.80	0.764	0.9325

Table 12

OP 300 Langmuir and Freundlich constants for methylene blue adsorption.

Langmuir isotherm coefficient			Freundlich isotherm coefficient		
q_m (mg/g)	K_L (L/mg)	R^2	K_F[(mg/g). (L/mg)$^{1/n}$]	1/n	R^2
30.57	0.381	0.47	6.62	0.530	0.65

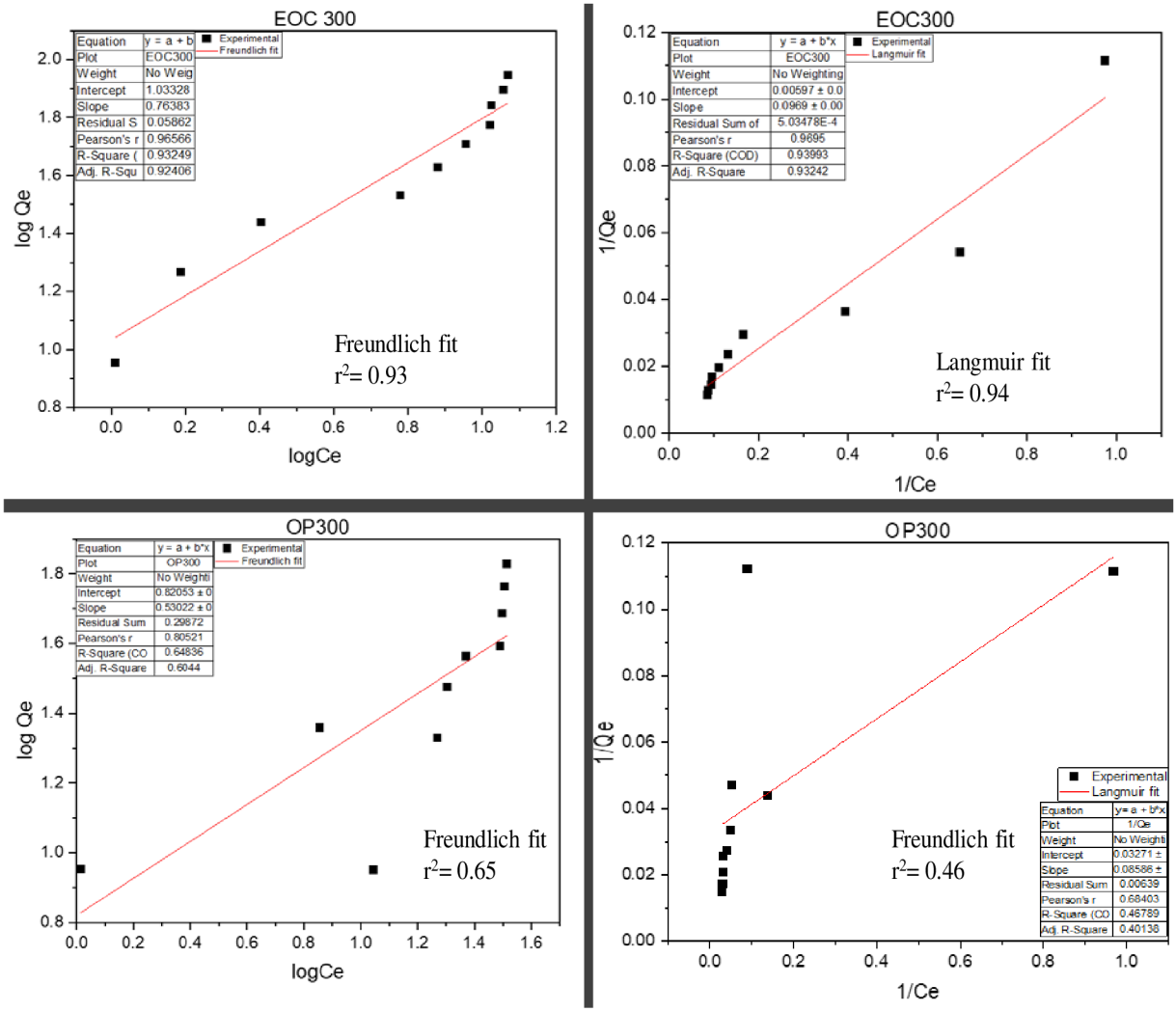

Figure 11 Adsorption isotherm(Freundlich & Langmuir) plot for EOC300 & OP300

6.3 Factors affecting the adsorption

6.3.1 Effect of adsorbate dose

The removal of Methylene blue was best described through Langmuir isotherm and the composite showed a maximum adsorption capacity of 167.50 mg/g, which was 5.5 fold more than the orange peel biochar. The initial Methylene blue (MB) concentration was kept in the range of 10-100 mg/l, whereas the adsorption capacity increased from 9 mg/g to 88 mg/g. As the initial concentration increased, the sorption potential also increased due to available adsorption sites, the maximum

removal efficiency of 92 % was achieved with the initial concentration of 20 mg/l and persisted constant with 84 % efficiency at initial concentration in between 40 to 70 mg/l.

6.3.2 Effect of interfering ions

The co-existence of different ions in textile wastewater may affect the adsorption of Methylene blue (Korenak et al., 2019). The effect of co-existing ions was investigated with different anions and cation, with initial concentration of 50 mg/l Methylene blue solution. The result has been mentioned in Figure No. 3, where it can be seen clearly that sulphate, nitrate, and chloride anions had little effect over adsorption capacity, where as sodium cation reduced the adsorption capacity from 42.09 mg/g to 35.09 mg/g. This behavior can be explained with sodium ion competing with dye for adsorption sites and resulted inhibitory effect for Methylene blue adsorption.

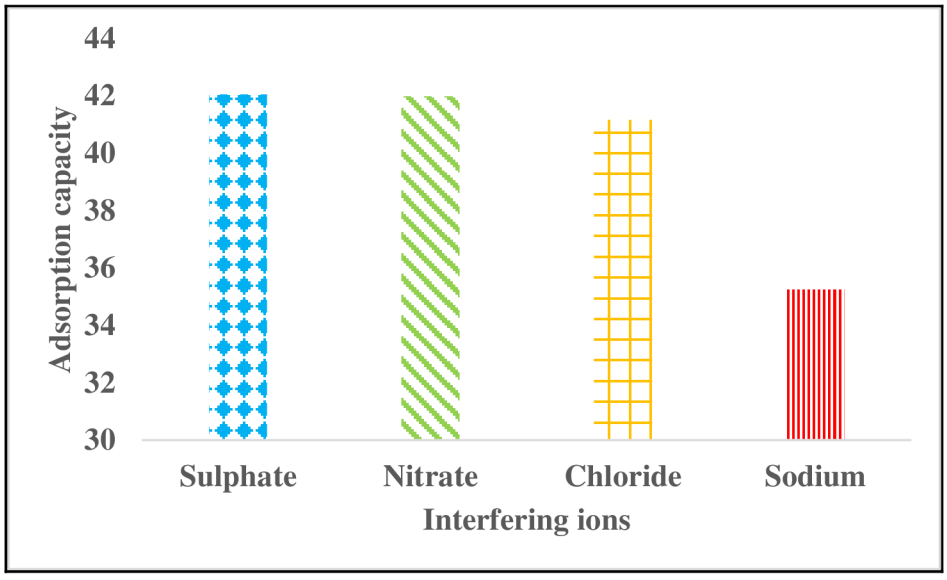

Figure12. Adsorption capacity with interfering ions

6.3.3 Solution pH

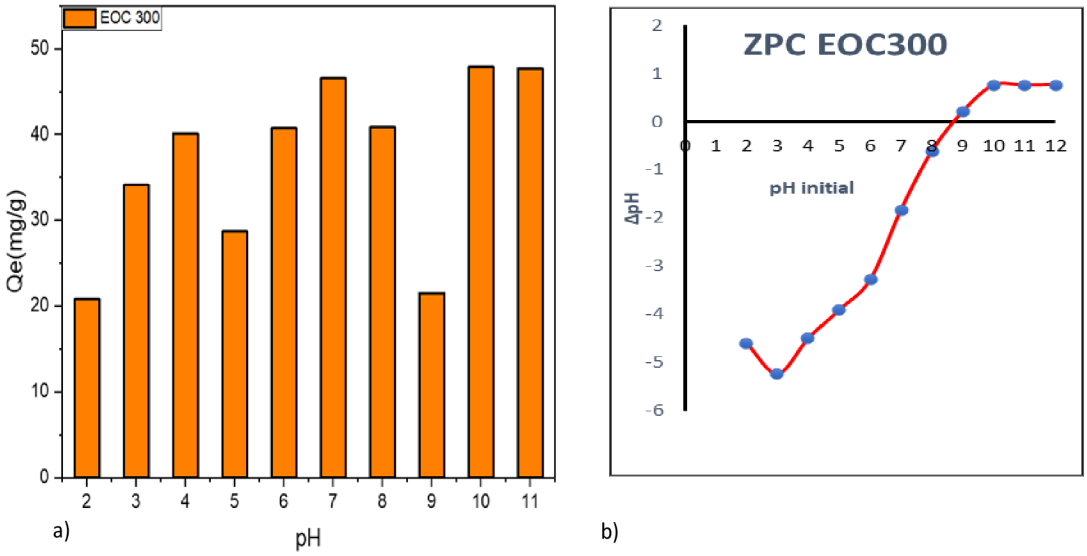

Fig.13 (a) Effect of pH on MB adsorption, (b)Zero point charge EOC300

The removal efficacy of composite was adequate to the different pH ranges and less affected by solution pH, adding advantage for its practical utility and promoting its potential use in a broad spectrum of environments. A maximum adsorption capacity of 47.90 mg/g was shown at pH value 10, and a minimum at pH 2 with an adsorption capacity of 20.80 mg/g. Comparatively, the adsorption capacity was less in an acidic medium due to methylene blue cations competing with H^+ ions for the sorption site and limiting composite efficiency(Liu et al.,2019; Weng et al., 2018). This adsorption mechanism was also explained by ZPC (pH), where it can be clearly seen at pH values of 10,11 and 12, the composite's surface charge becomes negative and promotes its higher efficiency for removing methylene blue.

7.1 OPC9 &OP9 COMPOSITE

7.1.1 SEM-EDX

The surface morphology and elemental composition were studied with SEM-EDX analysis. SEM images and EDS spectrum shown in Fig. confirm the porous morphology of the composite surface with enhanced graphitization with respect to unmodified orange peel biochar rectangular compartments-like structure. This methodology promotes the natural in-situ activation, with the release of CO_2 from the eggshell at 900^0C. Calcium carbonate, the main component of eggshell, decomposes at 900^0C, resulting in the formation of CaO and release of CO_2. Formation of CaO can also result in the specific decomposition of orange peel biomass. This novel methodology also establishes an effective interaction route of biomass and eggshell suspension extract, resulting in the formation of a highly porous surface with more mesoporous in nature. The EDX spectrum reveals rich element content with silicon percentage along with high oxygen elements, confirming the presence of different metal oxides. Silica percentage was enhanced with the modified orange peel with respect to the unmodified orange peel. Post-sorption deposition over pores can be clearly seen; after sorption, the carbon element weight percentage increased due to the presence of bisphenol-A, establishing the firm affinity of adsorbent towards the bisphenol-A.

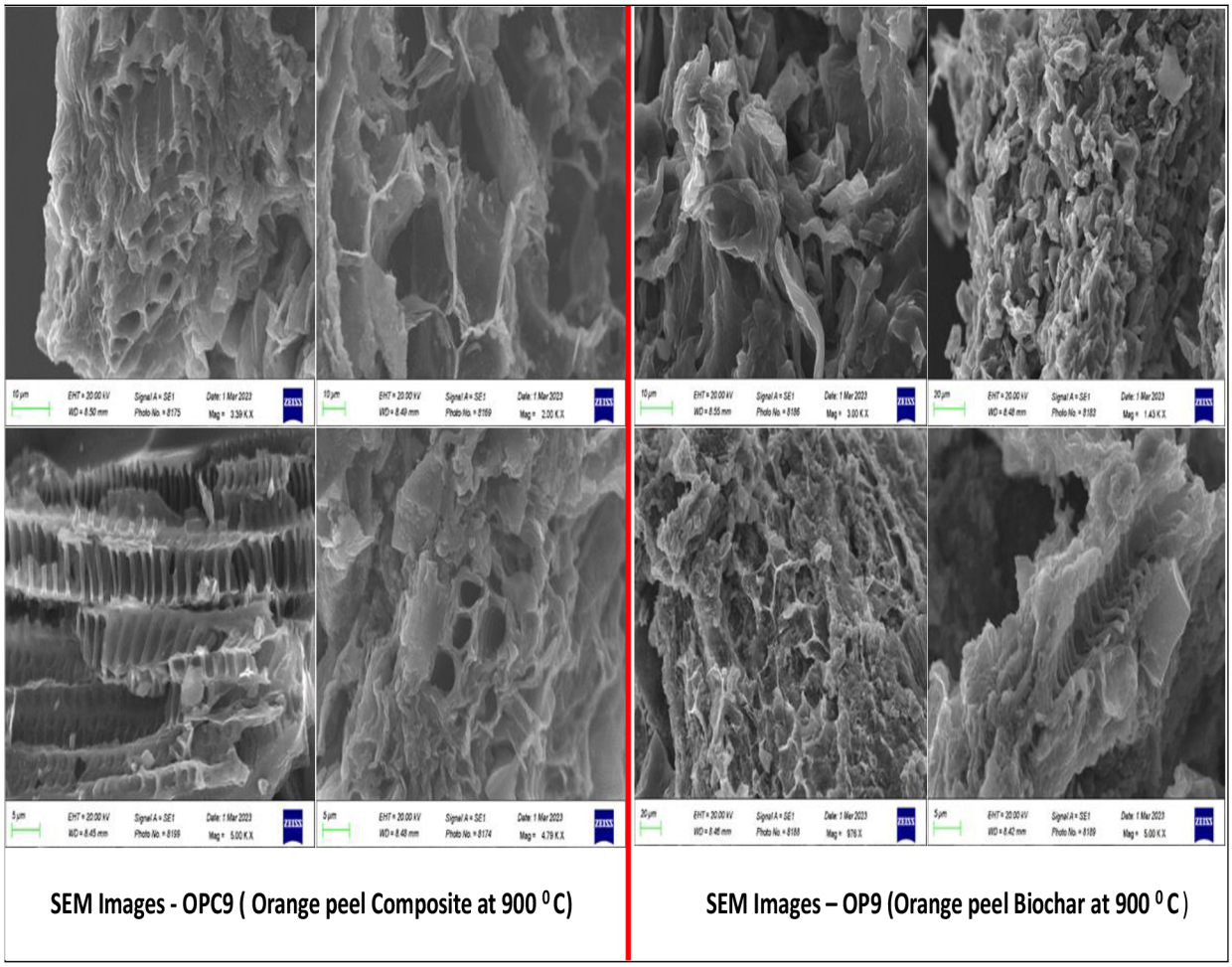

Fig.14 Comparison of the SEM images of the composite OPC9 & OP9

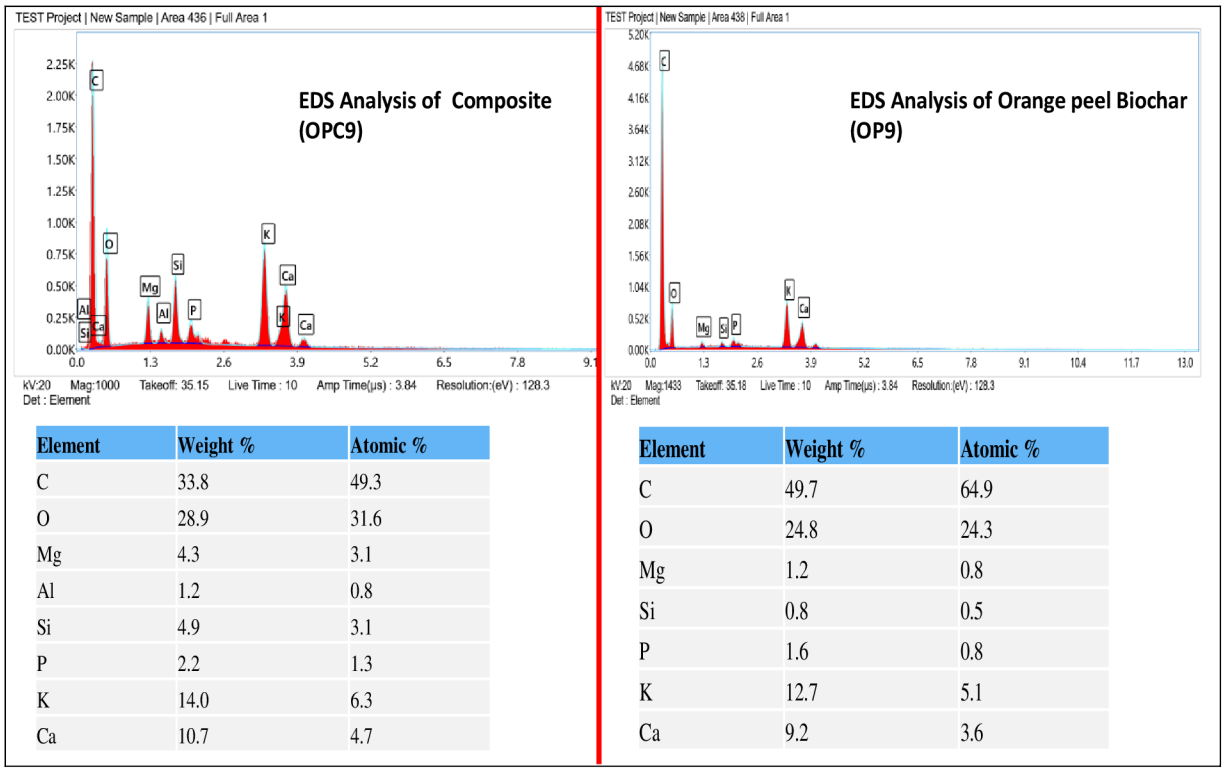

Element	Weight %	Atomic %
C	33.8	49.3
O	28.9	31.6
Mg	4.3	3.1
Al	1.2	0.8
Si	4.9	3.1
P	2.2	1.3
K	14.0	6.3
Ca	10.7	4.7

Element	Weight %	Atomic %
C	49.7	64.9
O	24.8	24.3
Mg	1.2	0.8
Si	0.8	0.5
P	1.6	0.8
K	12.7	5.1
Ca	9.2	3.6

Fig.15Comparison of EDS Analysis of the composite (OPC9) & Orange peel Biochar (OP9)

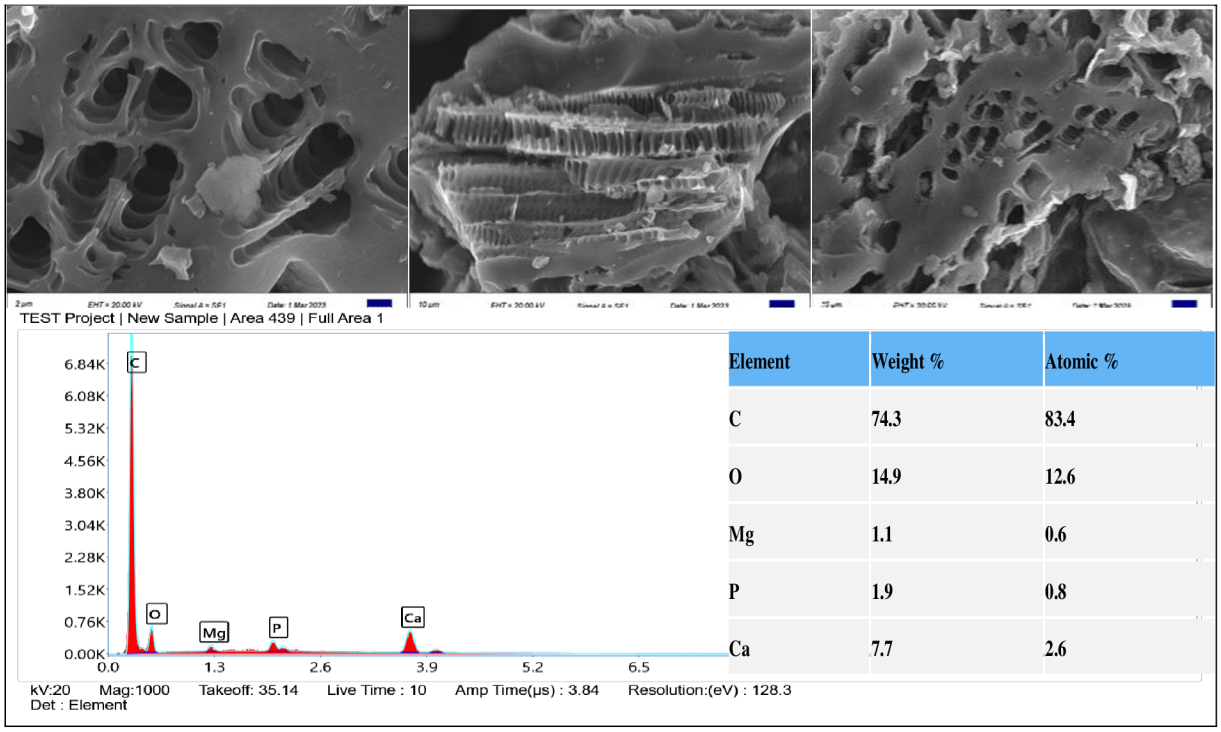

Element	Weight %	Atomic %
C	74.3	83.4
O	14.9	12.6
Mg	1.1	0.6
P	1.9	0.8
Ca	7.7	2.6

Fig.16 SEM-EDS Post-sorption analysis of the composite (OPC9)

7.1.2. XRD Analysis

The crystalline phase of the composite and orange peel biochar was studied with the XRD pattern in the range between 5^0 and 900 in the composite, which showed the typical major diffraction peak between 290 and $30^{0,}$ representing the presence of calcium oxide crystallinity. This pattern confirms the fusion of suspension eggshell to biomass with the designed methodology, and the intense crystalline

peak of calcium oxide shows a uniform presence in the carbonized skeleton. Silica peak at $23^{0.}$ This novel methodology proves to be successful in the fabrication of calcium oxide for composite formation. Diffraction peaks between 30^0 and 50^0 show different elements in oxide states. The broadness of the peak is more in orange peel biochar due to its amorphous nature. Eggshell modification helped to form more crystallinity in comparison to orange peel biochar. Pyrolysis at 900^0C led to the decomposition of calcium acetate and calcium carbonate to CaO with releasing of $CO_{2,}$ leading to a different mechanism of oxidation promoting a higher elemental oxidation state, eventually adding more crystallinity to the composite surface.

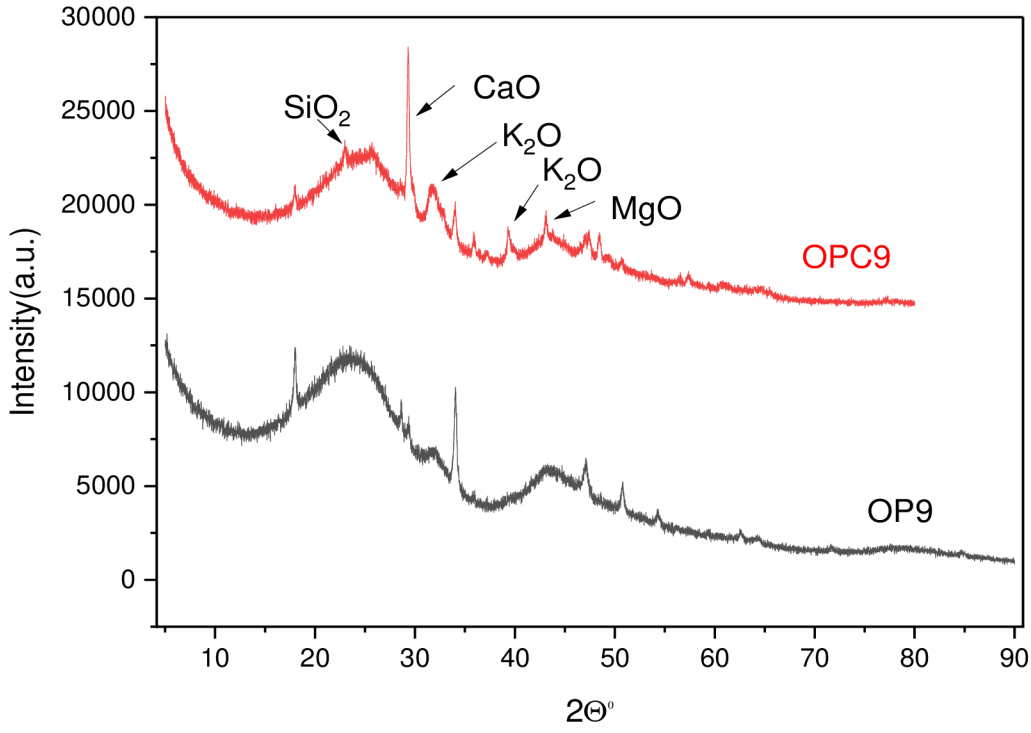

Fig.17. XRD Plot of the composite (OPC9) & Orange peel biochar (OP9)

7.1.3. FTIR Analysis

The composite and pristine biochar bonding pattern was investigated by FTIR spectroscopy in the range of 400 cm^{-1} to 4000 cm^{-1}. The pyrolysis was performed at 900^0C , so the presence of fundamental carbon skeleton C=O and C-O-C were present. The precipitation of calcium carbonate from eggshells has a different oxidation route. The composite showed distinctive peaks (fig. 6) at 874, 1050, and around 3000 $cm^{-1,}$ respectively, the peak at 874 cm^{-1}. The peak at 1050 cm^{-1}, correspondence to the C-O stretch

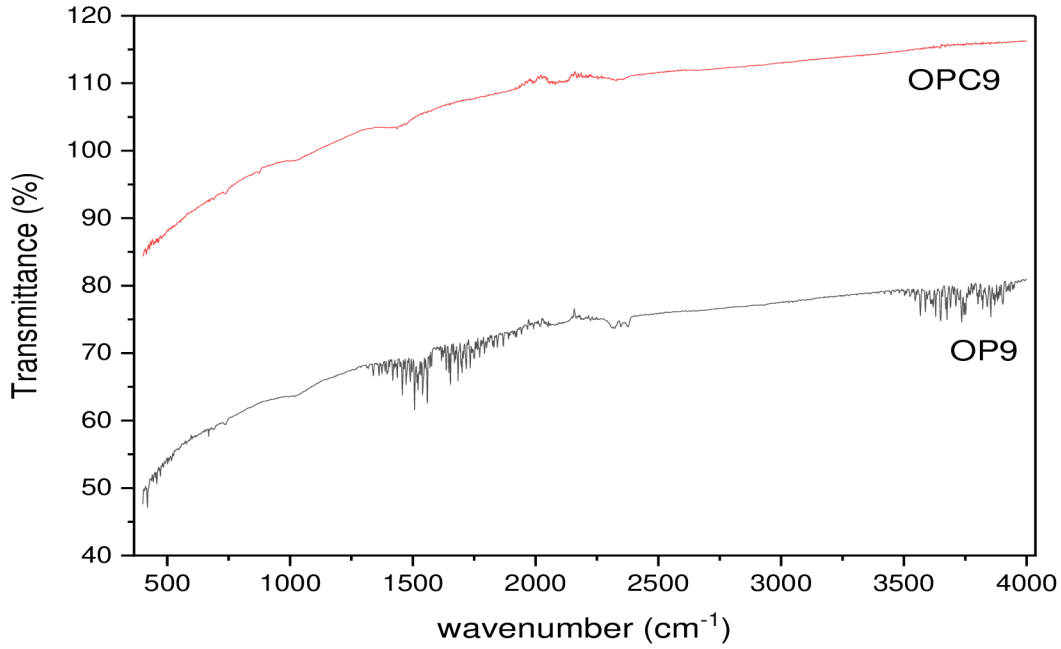

Fig. 18 FTIR spectrum of the composite (OPC9) & Orange peel biochar (OP9)

7.1.4 BET Analysis

The surface porosity of the orange peel biochar and orange peel composite was determined with nitrogen adsorption-desorption isotherm, as depicted in Fig. 4 (a) & (b); the obtained isotherms of the composite and pristine Biochar corresponds to the type I adsorption isotherm in IUPAC classification. The initial p/p_0 (below 0.01) rises steeply, marking the presence of micropores, and after that, the hysteresis loop begins from the range p/p_0 (0.1-0.9) showing mesoporous characteristics and at high p/p_0 (above 0.9) indicated steep rise marking the presence of macropores. The surface area of the orange peel biochar was 600 m^2, whereas the composite was 500 m^2, which was calculated using the BET equation. The difference in the surface could have contributed to the

formation of a successful composite with the modification, which did not affect the porosity to reduce the surface area of the composite. Even after modification, the porosity enhanced with the rise in pore volume due to the in situ CO_2 release with caco3 decomposition at 900 C. The initial novel modification with orange peel biomass and eggshell suspension at a particular temperature led to the successful precipitation of $CaCO_3$ over orange peel cellulosic content. Which strongly favored the formation of porous structures during carbonization at 900 C. The release of CO_2 also selected the different oxidation routes with other elements present within the biomass. The pore size analyses show that the majority of the pores are in the range of 0.5-2 nm, which belongs to the mesoporous category.

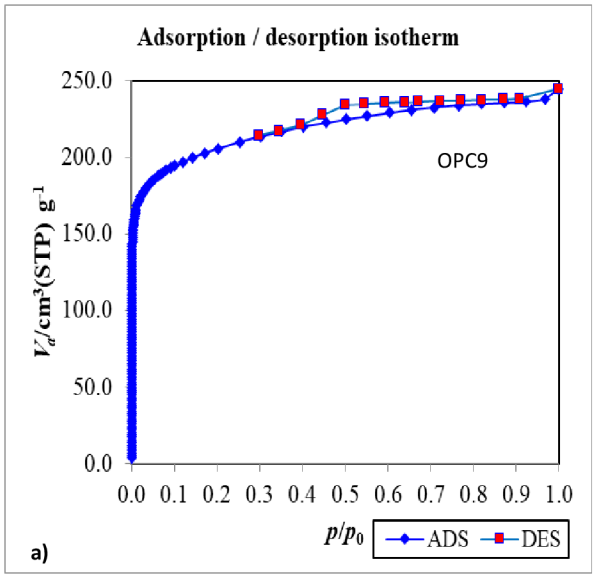

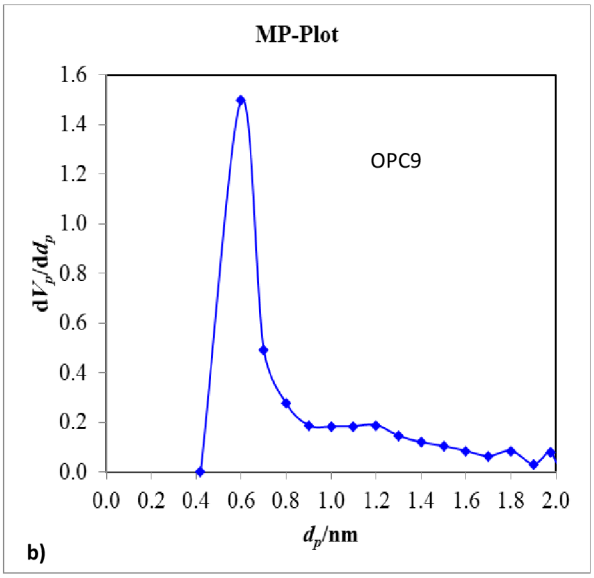

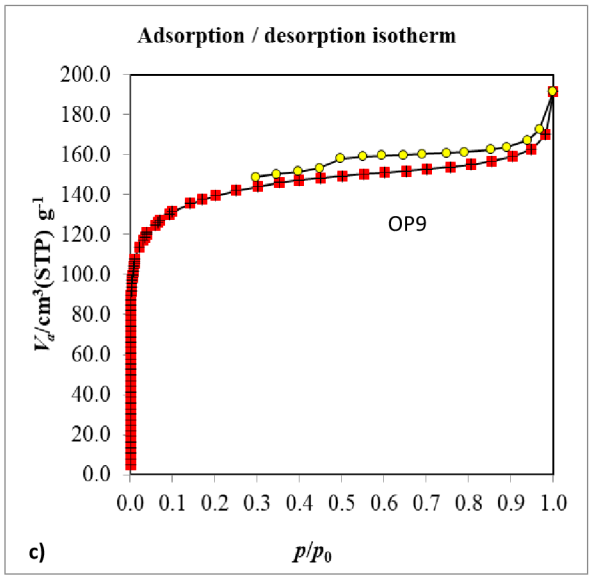

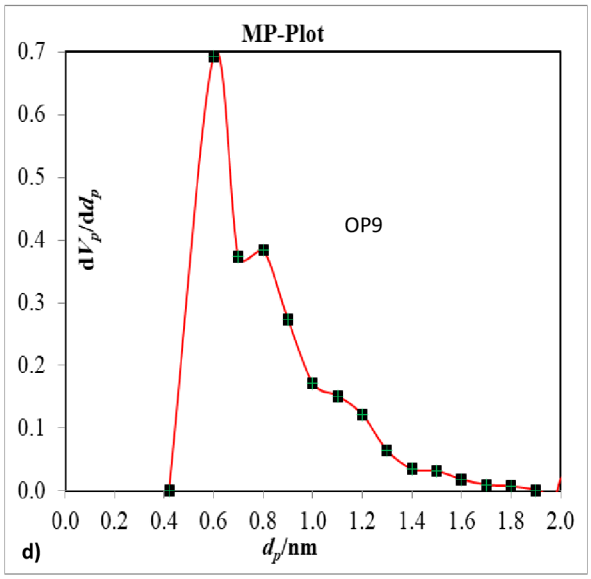

Fig.19.Adsorption isotherm & MP plot a &b for OPC9 , c & d for OP9

7.2 Experimental results

7.2.1 Adsorption mechanism

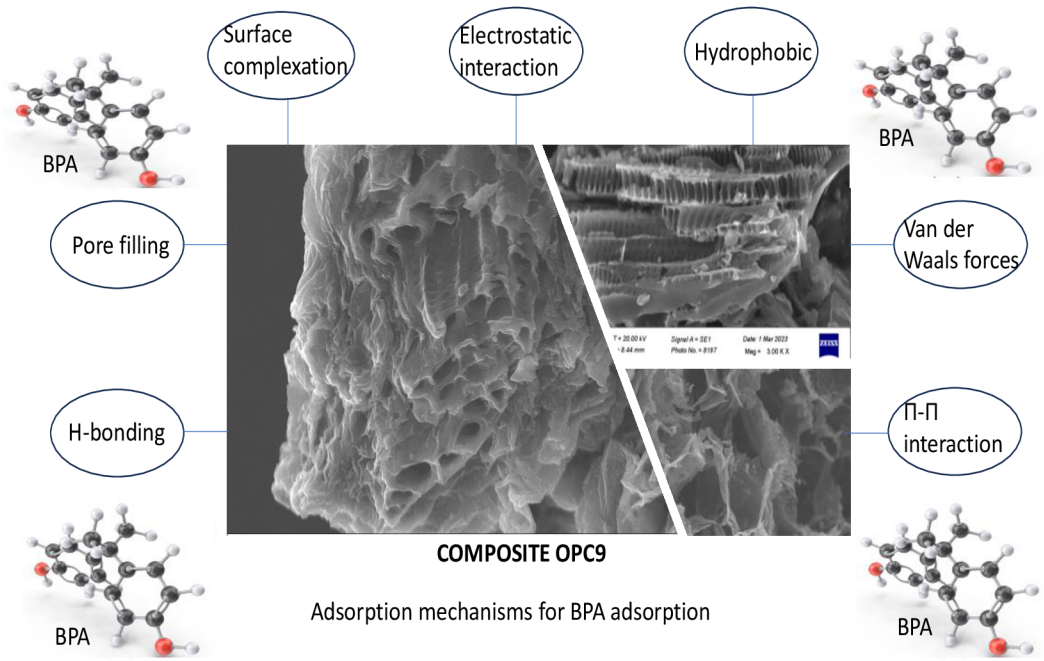

Fig.20 Adsorption mechanism for BPA removal

This novel technique maximized the effect of physisorption and chemisorption; the release of CO_2 during pyrolysis magnificently formed the pores, which facilitated the pore-filling of the BPA molecules and attracted Vander walls forces. The rich cationic surface composition with Ca, K, Si, Mg, and P enhanced the chemisorption and electrostatic attraction with modal pollutants. The increased percentage of oxygen supported the dipole interaction and hydrogen bonding. The pi bond in the composite, as well as in the BPA molecules, formed the pi-pi interaction for the adsorption. The hydrophobic nature of the BPA molecule also induced the sorption potential towards the composite surface.

7.2.2 Adsorption isotherm and kinetics modeling

The adsorption kinetics for the Bisphenol A removal mechanism were investigated with the pseudo-first-order (PFO) and pseudo-second-order (PSO) kinetic models, as well as the particle diffusion model. Pseudo-first-order and pseudo-second-order models were fitted with the experimental data.

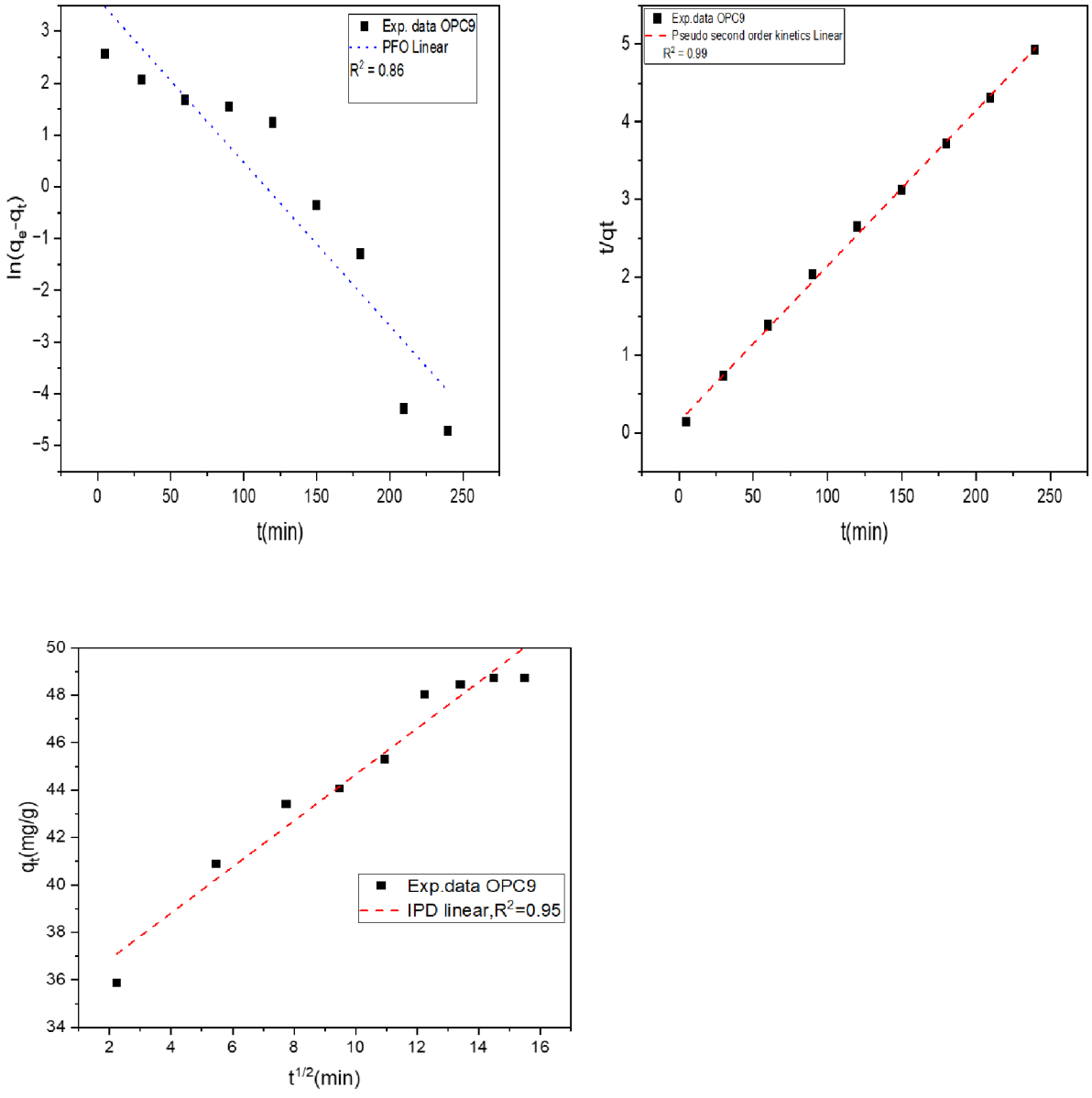

Fig.21 Plots for kinetic model

The initial concentration of the adsorbate was 50 mg/l, and the adsorption capacity increased with the progressive contact time. The experimental data was best fitted with the pseudo-second-order model, with a correlation coefficient (R^2 = 0.99) in comparison to PFO (R^2 = 0.86). The diffusion model was also studied for investigating the boundary layer diffusion condition, and experimental data showed a significant effect with the IPD model (R^2 = 0.95), marking the presence of physisorption, which could be supported with the porous structure in SEM images. This adsorption behavior showed the complex mechanism of both physisorption and chemisorption.

7.2.3 Adsorption isotherm

The adsorption mechanism of BPA under equilibrium state was examined at constant temperature with the isotherm models. In the current study, the Langmuir, Freundlich, and Temkin isotherm models were used to fit the experimental data. These models can reveal the interaction mechanism of adsorption.

Langmuir isotherm, an empirical model, assumes the monolayer and homogenous adsorption with a finite number of adsorption sites, and sites should have an equal affinity towards the adsorbate. Furthermore, it suggests that during adsorption, there is no interaction between the adsorbate and adsorbent surfaces. The linear form of the Langmuir isotherm equation can be expressed as follows:

Expression for the linear form of Langmuir equation:

$$1/q_e = 1/q_m K_L C_e + 1/ q_m \qquad (11)$$

Where C_e (mg L^{-1}) is the equilibrium concentration of BPA, q_e (mg g^{-1}) is the amount adsorbed by one gram of the adsorbent at equilibrium, q_m (mg g^{-1}) is the maximum monolayer adsorption capacity, K_L (L mg^{-1}) is the Langmuir isotherm constant.

Freundlich isotherm assumes a multilayer and heterogeneous adsorption system; affinities and heat of adsorption towards adsorbate molecules are not uniformly distributed on the surface of the adsorbent. Moreover, this isotherm depicts the chemisorption process. The expression for Freundlich isotherm is represented as follows:

Expression for the linear form of the Freundlich equation:

$$\text{Log } q_e = \log K_F + 1/n \log C_e \qquad (12)$$

where C_e (mg L^{-1}) is the equilibrium concentration of BPA, q_e (mg g^{-1}) is the amount adsorbed by one gram of the adsorbent at equilibrium, K_F [(mg g^{-1}) (L mg^{-1}), and n is the Freundlich isotherm constant.

The Temkin isotherm assumes a linear decrease of the heat of adsorption and ignores the extremely low and very high concentrations. This isotherm also assumes a uniform distribution of bounding energy with some maximum bonding energy. Temkin isotherm can be expressed as follows:

$$q_e = B\ln A + B\ln C_e \qquad (13)$$

where q_e (mg g^{-1}) is the amount of BPA adsorbed at equilibrium, C_e (mg L^{-1}) is the equilibrium concentration of BPA in solution. B is a constant related to the heat of adsorption and can be expressed as B – RT/b, b is the Temkin constant (J/mol), T is the absolute temperature (K), R is the gas constant (8.314 J/mol K), and A is the Temkin isotherm constant (L/g).

The experimental data showed mixed responses towards isotherm models and suggested complex adsorption mechanisms comprised of physisorption, chemisorption, and pore-filling adsorption controlling mechanisms. The maximum adsorption capacity of the composite (OPC9) was calculated with Langmuir isotherm 159 mg/g, whereas the maximum adsorption capacity of the Biochar (OP9) was reported 39.40 mg/g.

Table 13 Isotherm model fitting for OPC9 & OP9

Isotherm models (OPC9)	**R^2**	**Constants**
Temkin	0.78	At=1.95, Bt=37.56
Langmuir	0.77	Qm=159,KL=0.22
Freundlich	0.73	A=31.53, B=0.59

Isotherm model (OP9)	**R^2**	**Constants**
Langmuir	0.93	Max. Capacity, Qm=39.40

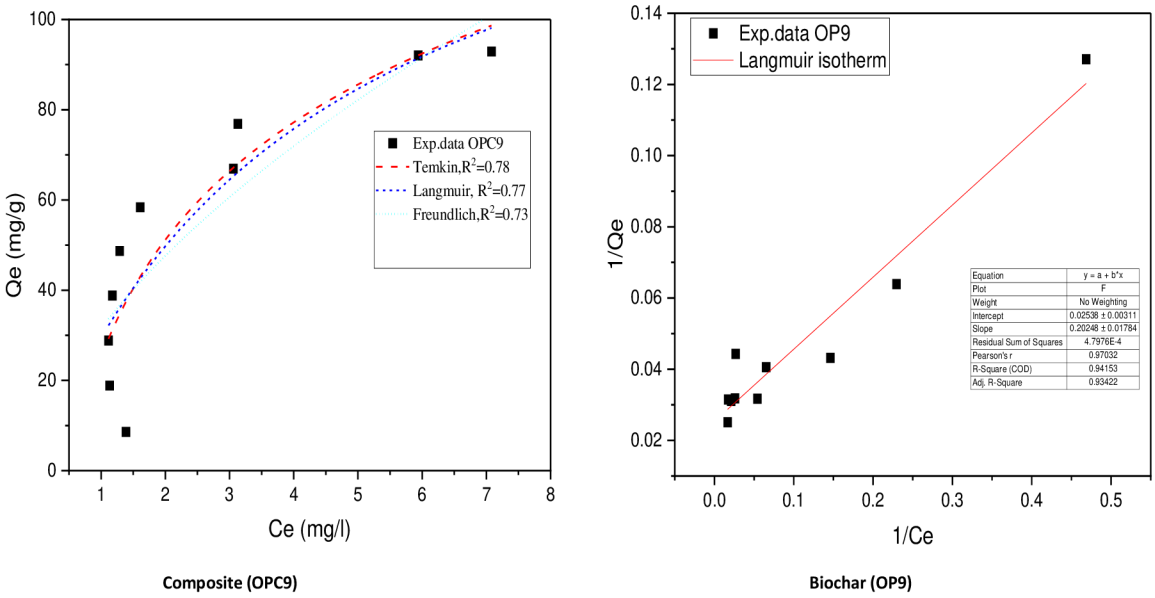

Fig. 22 Adsorption isotherm plot for OPC9 &OP9

The adsorption isotherm plot showed the complex mechanism of physisorption and chemisorption . The Temkin isotherm confirm the process of pore filling as an important mechanism for adsorption . The Langmuir and Freundlich isotherm state the physisorption with monolayer interaction and Freundlich isotherm depicted the chemical sorption with multilayer interaction.

7.3 Factors affecting the adsorption

7.3.1. Effect of pH

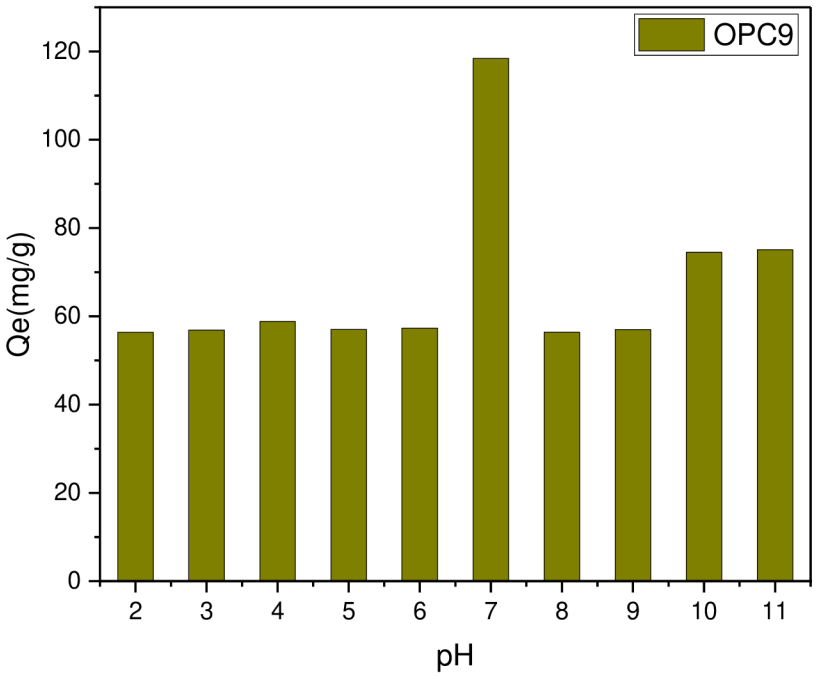

Fig.23 Effect of pH on BPA adsorption

The influence of the pH solution over adsorption efficiency was not significantly effective except at pH value 7 and slightly effective at pH 10 and 11. The pH_{zpc} value of the composite is 7; as clearly seen in an acidic environment, there is competition between positive cations present on the composite surface with H^+ ions, as cations present on the surface effectively form the surface complexation with the BPA. In the neutral medium, the surface of the composite showed better efficacy for surface complexation, eventually leading to better removal efficiency.

7.3.2. Effect of BPA initial concentration

The initial concentration effect of BPA on adsorption capacity was investigated, with initial concentration ranging from 20 to 200 ppm. As the initial concentration increased from 20 to 160 ppm, the adsorption capacity also increased from 18.88 to 158.97 mg/g, but the initial concentration increased from 160 ppm brings no to less change in the adsorption capacity confirms the saturation of the composite surface due to unavailability of the active sites.

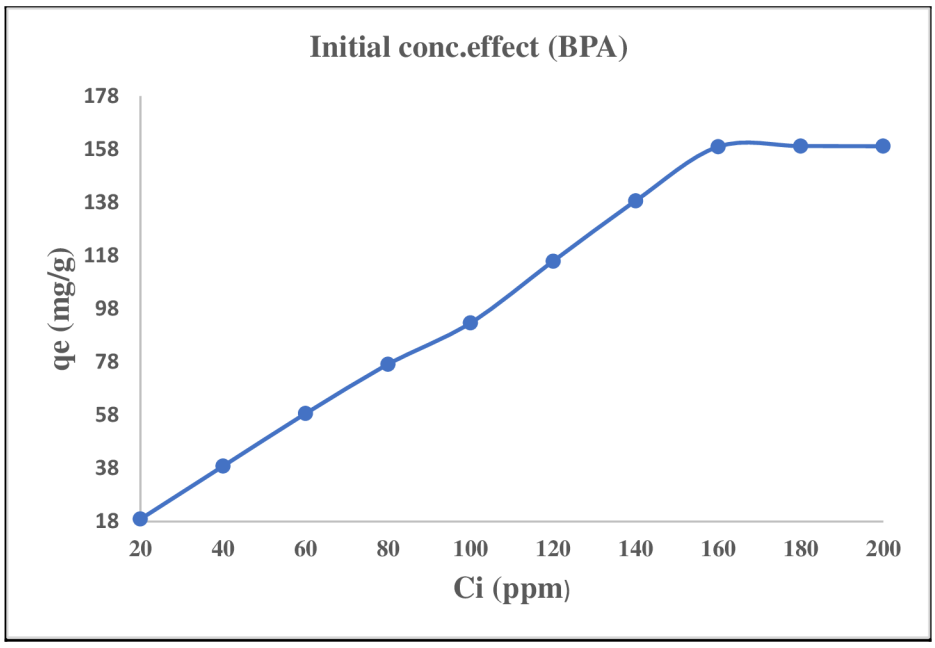

Fig.24 Effect of initial concentrations on BPA removal

3.10. Effect of the co-existing ions

The co-existence of different ions in an aqueous medium may affect the BPA adsorption; the effect of ionic strength was tested with different concentrations of NaCl. The initial concentration of BPA was 50 mg/l, whereas three different initial concentrations (mol L^{-1}) of 0.1, 0.2%, 0.3 %, 0.4%, and 0.5 mol L^{-1} of NaCl were taken for the investigation. The initial NaCl concentration reduced the adsorption capacity slightly, but as the concentration increased, the adsorption capacity also increased. This may be due to the increased concentration producing a screening effect of the surface charge that facilitated the Π-Π dispersion interaction and enhanced the adsorption of bisphenol A. Moreover, the salting-out effect could improve the BPA adsorption onto the composite.

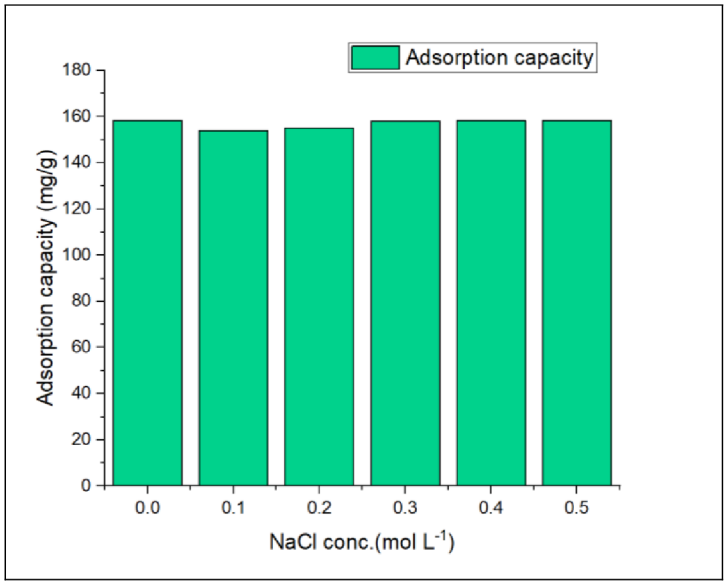

Fig. 25 Effect of co-existing ion on adsorption capacity

CHAPTER 6

Conclusion & Summary

4. Conclusion and Summary

This study gave the novel methodology for the synthesis of the green composite without generating a source of secondary pollutants to the environment. This methodology integrated the different environmental constraints with this common approach. This technique provided a natural fabrication methodology, which could open the door for different biomass modification process.

The functional composite EOC300 was prepared from the waste orange peel and chicken eggshell with the co-pyrolysis technique. The RSM tool was used to optimize the preparatory parameters through the Box-Behnken design, which provided the 17 experimental runs to perform. The best-optimized values of the selected input parameters resulted in the composite's higher adsorption efficiency. The eggshell acted as a source of natural in-situ activation during pyrolysis and increased the oxygenated functional groups over the composite surface. The EOC300 composite showed around 5.5-fold higher adsorption capacity for Methylene blue, along with 64 times higher surface area than unmodified orange peel. The adsorption behavior was perfectly explained with the Langmuir isotherm model showing a maximum adsorption capacity of 167mg/g, where as composite OPC9 showed highly well developed porous structure with large surface area, which showed the 100 % removal efficiency of BPA with maximum adsorption capacity of 159 mg/g. This study also provided a new fabrication technique without chemical modification also reduced the source for secondary pollutants, while synthesis. This investigation integrated the different environmental constraints and addressed them simultaneously. This green sorbent can treat a wide rang of organic contaminants due to its effective physicochemical properties.

PART VI

Bibliography & references

Bibliography

W John Thomas, F., & Crittenden, B. (1998). Adsorption technology and design. Butterworth-Heinemann.

Ali, I., & Gupta, V. K. (2006). Advances in water treatment by adsorption technology. Nature protocols, 1(6), 2661-2667.

Pourhakkak, P., Taghizadeh, A., Taghizadeh, M., Ghaedi, M., & Haghdoust, S. (2021). Fundamentals of adsorption technology. In Interface Science and Technology (Vol. 33, pp. 1-70). Elsevier.

Worch, E. (2021). Adsorption technology in water treatment: fundamentals, processes, and modeling. Walter de Gruyter GmbH & Co KG.

Barceló, D. (Ed.). (2012). Emerging organic contaminants and human health (Vol. 20). Springer.

Chiou, C. T. (2003). Partition and adsorption of organic contaminants in environmental systems. John Wiley & Sons.

Rao, P. S. C. (1990). Sorption of organic contaminants. Water science and technology, 22(6), 1-6.

Faust, S. D., & Aly, O. M. (2013). Adsorption processes for water treatment. Elsevier.

Grassi, M., Kaykioglu, G., Belgiorno, V., & Lofrano, G. (2012). Removal of emerging contaminants from water and wastewater by adsorption process. Emerging compounds removal from wastewater: natural and solar based treatments, 15-37.

Summers, R. S., Knappe, D. R., & Snoeyink, V. L. (2011). Adsorption of organic compounds by activated carbon. Water quality and treatment: A handbook on drinking water, 6th Edition. Edited by JK Edzwald. McGraw-Hill.

References

1. Abd El-Monaem, Omer, A.M., El-Subruiti, M. (2022). Zero-valent iron supported-lemon derived biochar for ultra-fast adsorption of methylene blue. Biomass Conv. Bioref. https://doi.org/10.1007/s13399-022-02362-y
2. Abdelaal, A., Pradhan, S., AlNouss, A., Tong, Y., Al-Ansari, T., McKay, G., & Mackey, H. R. (2021). The impact of pyrolysis conditions on orange peel biochar physicochemical properties for sandy soil. *Waste management & research : the journal of the International Solid Wastes and Public Cleansing Association, ISWA*, *39*(7), 995–1004. https://doi.org/10.1177/0734242X20978456.
3. Abdelfatah, A. M., Fawzy, M., Eltaweil, A. S., & El-Khouly, M. E. (2021). Green synthesis of nano-zero-valent iron using ricinus communis seeds extract: Characterization and application in the treatment of methylene blue-polluted water. *ACS omega*, *6*(39), 25397-25411.
4. Aboagye, D., Banadda, N., Kiggundu, N., Kabenge, I. (2017). Assessment of orange peel waste availability in ghana and potential bio-oil yield using fast pyrolysis. Renewable and Sustainable Energy Reviews, 70, 814-821. https://doi.org/10.1016/j.rser.2016.11.262.
5. Ahmad, A., Singh, A.P., Khan, N., Chowdhary, P., Giri, B.S., Varjani, S., Chaturvedi, P. (2021). Bio-composite of Fe-sludge biochar immobilized with Bacillus Sp. in packed column for bio-adsorption of Methylene blue in a hybrid treatment system: Isotherm and kinetic evaluation. Environmental Technology & Innovation, 23, 101734. https://doi.org/10.1016/j.eti.2021.101734.

6. Ali, I. & Jain, C.K. in Water Encyclopedia: Domestic, municipal, and industrial water supply and waste disposal (ed. Lehr, J.)(John Wiley & Sons, New York, 2005).
7. Al-Tohamy, R., Ali, S. S., Li, F., Okasha, K. M., Mahmoud, Y. A. G., Elsamahy, T., ... & Sun, J. (2022). A critical review on the treatment of dye-containing wastewater: Ecotoxicological and health concerns of textile dyes and possible remediation approaches for environmental safety. *Ecotoxicology and Environmental Safety*, *231*, 113160.
8. Amin, M. T., Alazba, A. A., & Shafiq, M. (2019). Comparative study for adsorption of methylene blue dye on biochar derived from orange peel and banana biomass in aqueous solutions. *Environmental monitoring and assessment*, *191*(12), 735. https://doi.org/10.1007/s10661-019-7915-0
9. Anandan, S., Ponnusamy, V. K., & Ashokkumar, M. (2020). A review on hybrid techniques for the degradation of organic pollutants in aqueous environment. *Ultrasonics Sonochemistry*, *67*, 105130.
10. Andersen, J. K., Boldrin, A., Christensen, T. H., & Scheutz, C. (2010). Greenhouse gas emissions from home composting of organic household waste. *Waste management (New York, N.Y.)*, *30*(12), 2475–2482. https://doi.org/10.1016/j.wasman.2010.07.004.
11. Aworn, A., Thiravetyan, P., & Nakbanpote, W. (2008). Preparation and characteristics of agricultural waste activated carbon by physical activation having micro-and mesopores. *Journal of Analytical and Applied Pyrolysis*, *82*(2), 279-285. https://doi.org/10.1016/j.jaap.2008.04.007
12. Bai, Y., & Hong, J. (2021). Preparation of a Novel Millet Straw Biochar-Bentonite Composite and Its Adsorption Property of Hg^{2+} in Aqueous Solution. *Materials (Basel, Switzerland)*, *14*(5), 1117. https://doi.org/10.3390/ma14051117.

13. Bao, D., Li, Z., Tang, R., Wan, C., Zhang, C., Tan, X., & Liu, X. (2021). Metal-modified sludge-based biochar enhances catalytic capacity: Characteristics and mechanism. *Journal of Environmental Management*, *284*, 112113. https://doi.org/10.1016/j.jenvman.2021.112113

14. Cha, J. S., Choi, J. C., Ko, J. H., Park, Y. K., Park, S. H., Jeong, K. E., ... & Jeon, J. K. (2010). The low-temperature SCR of NO over rice straw and sewage sludge derived char. *Chemical Engineering Journal*, *156*(2), 321-327. https://doi.org/10.1016/j.cej.2009.10.027

15. Chiou, J. R., Lai, B. H., Hsu, K. C., & Chen, D. H. (2013). One-pot green synthesis of silver/iron oxide composite nanoparticles for 4-nitrophenol reduction. *Journal of hazardous materials*, *248*, 394-400.

16. Cui, X., Wang, J., Wang, X., Khan, M. B., Lu, M., Khan, K. Y., Song, Y., He, Z., Yang, X., Yan, B., & Chen, G. (2022). Biochar from constructed wetland biomass waste: A review of its potential and challenges. *Chemosphere*, *287*(Pt 3), 132259.https://doi.org/10.1016/j.chemosphere.2021.132259.

17. Cui, X., Zhang, S. S., Geng, Y., Zhen, J., Zhan, J., Cao, C., & Ni, S. Q. (2021). Synergistic catalysis by Fe3O4-biochar/peroxymonosulfate system for the removal of bisphenol a. *Separation and Purification Technology*, *276*, 119351.

18. Darvishi, A., & Bakhshi, H. (2016). Poly(sodium methacrylate)/eggshell particles hydrogel composites as dye sorbent. *Water science and technology : a journal of the International Association on Water Pollution Research*, *74*(12), 2807–2818. https://doi.org/10.2166/wst.2016.453.

19. Diao, Z. H., Dong, F. X., Yan, L., Chen, Z. L., Qian, W., Kong, L. J., ... & Chu, W. (2020). Synergistic oxidation of Bisphenol A in a heterogeneous ultrasound-enhanced sludge

biochar catalyst/persulfate process: Reactivity and mechanism. *Journal of hazardous materials*, *384*, 121385. https://doi.org/10.1016/j.jhazmat.2019.121385.

a. doi:10.1021/jf073388r

20. Dzoujo, H.M., Shikuku, V. O., Tome, S., Akiri, S., Kengne, N.M., Abdpour, S., Janiak, C., Etoh, M.A., Dina, D.(2022). Synthesis of pozzolan and sugarcane bagasse derived geopolymer-biochar composites for methylene blue sequestration from aqueous medium.Journal of Environmental Management, 318, 115533. https://doi.org/10.1016/j.jenvman.
21. Eskikaya, O., Gun, M., Bouchareb, R., Bilici, Z., Dizge, N., Ramaraj, R., & Balakrishnan, D. (2022). Photocatalytic activity of calcined chicken eggshells for Safranin and Reactive Red180decolorization. *Chemosphere*, *304*,135210.https://doi.org/10.1016/j.chemosphere.2022.135210.
22. Fan, J., Li, Y., Yu, H., Li, Y., Yuan, Q., Xiao, H., Li, F., & Pan, B. (2020). Using sewage sludge with high ash content for biochar production and Cu(II) sorption. *The Science of the total environment*, *713*, 136663. https://doi.org/10.1016/j.scitotenv.2020.136663.
23. Faust, S.D. & Aly, O.M. Chemistry of water treatment (Butterworth, Stoneham, Massachusetts, 1983).
24. Gan, L., Fang, X., Xu, L., Wang, L., Wu, Y., Dai, B., ... & Shi, J. (2021). Boosted activity of δ-MnO2 by Kenaf derived carbon fiber for high-efficient oxidative degradation of bisphenol A in water. *Materials & Design*, *203*, 109596.
25. Ghaly, A. E., Ananthashankar, R., Alhattab, M. V. V. R., & Ramakrishnan, V. V. (2014). Production, characterization and treatment of textile effluents: a critical review. *J Chem Eng Process Technol*, *5*(1), 1-19.

26. Girotto, F., Alibardi, L., & Cossu, R. (2015). Food waste generation and industrial uses: A review. *Waste management (New York, N.Y.)*, *45*, 32–41. https://doi.org/10.1016/j.wasman.2015.06.008.

27. Goeury, K., Munoz, G., Duy, S. V., Prévost, M., & Sauvé, S. (2022). Occurrence and seasonal distribution of steroid hormones and bisphenol A in surface waters and suspended sediments of Quebec, Canada. *Environmental Advances*, *8*, 100199.

28. Gopinath, A., Divyapriya, G., Srivastava, V., Laiju, A. R., Nidheesh, P. V., & Kumar, M. S. (2021). Conversion of sewage sludge into biochar: A potential resource in water and wastewater treatment. *Environmental Research*, *194*, 110656. https://doi.org/10.1016/j.envres.2020.110656.

29. Grassi, M., Kaykioglu, G., Belgiorno, V., & Lofrano, G. (2012). Removal of emerging contaminants from water and wastewater by adsorption process. In G. Lofrano (Ed.), Emerging Compounds Removal from Wastewater (pp. 15–37). Dordrecht: Springer Netherlands. https://doi.org/10.1007 /978-94-007-3916-1_2.

30. Guediri, A., Bouguettoucha, A., Chebli, D., Chafai, N., & Amrane, A. (2019). Molecular dynamic simulation and DFT computational studies on the adsorption performances of methylene blue in aqueous solutions by orange peel-modified phosphoric acid. Journal of Molecular Structure, 1202, 127290. https://doi.org/10.1016/j.molstruc.2019.127290.

31. Hengstler, J. G., Foth, H., Gebel, T., Kramer, P. J., Lilienblum, W., Schweinfurth, H., ... & Gundert-Remy, U. (2011). Critical evaluation of key evidence on the human health hazards of exposure to bisphenol A. *Critical reviews in toxicology*, *41*(4), 263-291.

32. Heo, J., Yoon, Y., Lee, G., Kim, Y., Han, J., & Park, C. M. (2019). Enhanced adsorption of bisphenol A and sulfamethoxazole by a novel magnetic CuZnFe2O4–biochar composite. *Bioresource Technology*, *281*, 179-187.

33. Hong, S. H., Lyonga, F. N., Kang, J. K., Seo, E. J., Lee, C. G., Jeong, S., Hong, S. G., & Park, S. J. (2020). Synthesis of Fe-impregnated biochar from food waste for Selenium(VI) removal from aqueous solution through adsorption: Process optimization and assessment. *Chemosphere*, *252*, 126475. https://doi.org/10.1016/j.chemosphere.2020.126475.

    a. https://doi.org/10.1016/j.jiec.2018.03.027.

34. Igalavithana, A. D., Choi, S. W., Dissanayake, P. D., Shang, J., Wang, C. H., Yang, X., Kim, S., Tsang, D. C. W., Lee, K. B., & Ok, Y. S. (2020). Gasification biochar from biowaste (food waste and wood waste) for effective CO_2 adsorption. *Journal of hazardous materials*, *391*, 121147. https://doi.org/10.1016/j.jhazmat.2019.121147.

35. Igalavithana, A. D., Lee, S. E., Lee, Y. H., Tsang, D. C. W., Rinklebe, J., Kwon, E. E., & Ok, Y. S. (2017). Heavy metal immobilization and microbial community abundance by vegetable waste and pine cone biochar of agricultural soils. *Chemosphere*, *174*, 593–603. https://doi.org/10.1016/j.chemosphere.2017.01.148.

36. Iqbal, J., Shah, N. S., Sayed, M., Niazi, N. K., Imran, M., Khan, J. A., Khan, Z. U. H., Hussien, A. G. S., Polychronopoulou, K., & Howari, F. (2021). Nano-zerovalent manganese/biochar composite for the adsorptive and oxidative removal of Congo-red dye from aqueous solutions. *Journal of hazardous materials*, *403*, 123854. https://doi.org/10.1016/j.jhazmat.2020.123854.

37. Jang, H. M., & Kan, E. (2019). Engineered biochar from agricultural waste for removal of tetracycline in water. *Bioresource technology*, *284*, 437–447. https://doi.org/10.1016/j.biortech.2019.03.131.

38. Jayawardhana, Y., Gunatilake, S. R., Mahatantila, K., Ginige, M. P., & Vithanage, M. (2019). Sorptive removal of toluene and m-xylene by municipal solid waste biochar:

Simultaneous municipal solid waste management and remediation of volatile organic compounds. *Journal of Environmental Management*, *238*, 323–330. https://doi.org/10.1016/j.jenvman.2019.02.097.

39. Jiang, S. F., Ling, L. L., Chen, W. J., Liu, W. J., Li, D. C., & Jiang, H. (2019). High efficient removal of bisphenol A in a peroxymonosulfate/iron functionalized biochar system: mechanistic elucidation and quantification of the contributors. *Chemical Engineering Journal*, *359*, 572-583.
40. Journal of Hazardous Materials
41. Kebaili, M., Djellali, S., Radjai, M., Drouiche, N., Lounici, H. (2018). Valorization of orange industry residues to form a natural coagulant and adsorbent. 6464Journal of Industrial and Engineering Chemistry, 64, 292-299.
42. Korenak, J., Helix-Nielsen, C., Buksek, Petrinic, I. (2019). Efficiency and economic feasibility of forward osmosis in textile wastewater treatment. Journal of cleaner production, 210, 1483-1495. https://doi.org/10.1016/j.jclepro.2018.11.130.
43. Kuan, J., Zhang, H., Gu, H., Zhang, Y., Wu, H., & Mao, N. (2022). Adsorption-enhanced photocatalytic property of Ag-doped biochar/g-C3N4/TiO2 composite by incorporating cotton-based biochar. *Nanotechnology*, 10.1088/1361-6528/ac705e. Advance online publication. https://doi.org/10.1088/1361-6528/ac705e.
44. Kumar, N., Vach, M., Saini, V. K., & Zitkova, A. (2024). Co-pyrolysis of orange peel and eggshell for oxygenated rich composite: Process optimization with response surface methodology. *Journal of Environmental Management*, *351*, 119786.
45. Kumar, R., Adhikari, S., Driver, E., Zevitz, J., & Halden, R. U. (2022). Application of wastewater-based epidemiology for estimating population-wide human exposure to -

ohthalate esters, bisphenols, and terephthalic acid. *Science of the Total Environment*, *847*, 157616.

46. Laca, A., Laca, A., & Díaz, M. (2017). Eggshell waste as catalyst: A review. *Journal of Environmental Management*, *197*, 351–359. https://doi.org/10.1016/j.jenvman.2017.03.088.

47. Li, W., Mu, B., & Yang, Y. (2019). Feasibility of industrial-scale treatment of dye wastewater via bio-adsorption technology. *Bioresource technology*, *277*, 157–170. https://doi.org/10.1016/j.biortech.2019.01.002.

48. Li, Y., Wang, L.E., Liu, G., Cheng, S.(2021). Rural household food waste characteristics and driving factors in China, 164,105209. https://doi.org/10.1016/j.resconrec.2020.105209.

49. Liu, H., Zhu, J., Li, Q., Li, L., Huang, Y., Wang, Y., Fan, G., Zhang, L. (2023). Adsorption Performance of Methylene Blue by KOH/FeCl3 Modified Biochar/Alginate Composite Beads Derived from Agricultural Waste. Molecules, 28, 2507. https://doi.org/10.3390/molecules28062507

50. Liu, X., Shen, F., & Qi, X. (2019). Adsorption recovery of phosphate from aqueous solution by CaO-biochar composites prepared from eggshell and rice straw. *Science of the total environment*, *666*, 694-702.

51. Liu, Y., Chen, Y., Li, Y., Chen, L., Jiang, H., Li, H., Luo, X., Tang, P., Yan, H., Zhao, M., Yuan, Y., & Hou, S. (2022). Fabrication, application, and mechanism of metal and heteroatom co-doped biochar composites (MHBCs) for the removal of contaminants in water: A review. *Journal of hazardous materials*, *431*, 128584. https://doi.org/10.1016/j.jhazmat.2022.128584

52. Liu, Z., Yang, S., Zhang, L., Zeng, J., Tian, S., & Lin, Y. (2022). The Removal of Pb^{2+} from Aqueous Solution by Using Navel Orange Peel Biochar Supported Graphene Oxide:

Characteristics, Response Surface Methodology, and Mechanism. *International journal of environmental research and public health*, *19*(8), 4790. https://doi.org/10.3390/ijerph19084790.

53. Lorestani, F., Shahnavaz, Z., Mn, P., Alias, Y., & Manan, N. S. (2015). One-step hydrothermal green synthesis of silver nanoparticle-carbon nanotube reduced-graphene oxide composite and its application as hydrogen peroxide sensor. *Sensors and Actuators B: Chemical*, *208*, 389-398.
54. Luo, Y., Han, Y., Xue, M., Xie, Y., Yin, Z., Xie, C., Li, X., Zheng, Y., Huang, J., Zhang, Y., Yang, Y., & Gao, B. (2022). Ball-milled bismuth oxybromide/biochar composites with enhanced removal of reactive red owing to the synergy between adsorption and photodegradation. *Journal of environmental management*, *308*, 114652. https://doi.org/10.1016/j.jenvman.2022.114652.
55. Ma, Y., Liu, H., Wu, J., Yuan, L., Wang, Y., Du, X., ... & Zhang, H. (2019). The adverse health effects of bisphenol A and related toxicity mechanisms. *Environmental research*, *176*, 108575.
56. Madima, N., Mishra, S.B., Inamuddin, I., Mishra, A.K.(2020). Carbon-based nanomaterials for remediatins of organic and inorganic pollutants from wastewater. A review. Environmental Chemistry Letters 18, 1169-1191.
57. Manfredi, S., Tonini, D., Christensen, T. H., & Scharff, H. (2009). Landfilling of waste: accounting of greenhouse gases and global warming contributions. *Waste management & research : the journal of the International Solid Wastes and Public Cleansing Association, ISWA*, *27*(8), 825–836. https://doi.org/10.1177/0734242X09348529.
58. Marium Waheed, Muhammad Yousaf, Aamir Shehzad, Muhammad Inam-Ur-Raheem, Muhammad Kashif Iqbal Khan, Moazzam Rafiq Khan, Naveed Ahmad, Abdullah, Rana

Muhammad Aadil, Channelling eggshell waste to valuable and utilizable products: A comprehensive review,Trends in Food Science & Technology,Volume 106,2020,Pages 78-90,ISSN 0924-2244, https://doi.org/10.1016/j.tifs.2020.10.009.

59. Mestre, A. S., Pires, J., Nogueira, J. M. F., & Carvalho, A. P. (2007). Activated carbons for the adsorption of ibuprofen. *Carbon*, *45*(10), 1979-1988. https://doi.org/10.1016/j.carbon.2007.06.005

60. Nakagawa, Y., Molina-Sabio, M., & Rodríguez-Reinoso, F. (2007). Modification of the porous structure along the preparation of activated carbon monoliths with H3PO4 and ZnCl2. *Microporous and Mesoporous Materials*, *103*(1-3), 29-34. https://doi.org/10.1016/j.micromeso.2007.01.029

61. Nguyen, V. T., Vo, T. D., Nguyen, T. B., Dat, N. D., Huu, B. T., Nguyen, X. C., Tran, T., Le, T. N., Duong, T. G., Bui, M. H., Dong, C. D., & Bui, X. T. (2022). Adsorption of norfloxacin from aqueous solution on biochar derived from spent coffee ground: Master variables and response surface method optimized adsorption process. *Chemosphere*, *288*(Pt 2), 132577. https://doi.org/10.1016/j.chemosphere.2021.132577.

62. Özsin, G., Kılıç, M., Apaydın-Varol, E., & Pütün, A. E. (2019). Chemically activated carbon production from agricultural waste of chickpea and its application for heavy metal adsorption: equilibrium, kinetic, and thermodynamic studies. *Applied water science*, *9*, 1-14.

63. Paggiola, G., Stempvoort, S.V., Bustamante, J., Barbero, J.M.V., Hunt, A.J., Clark, J.H. (2016). Can bio-based chemicals meet demand? Global and regional case-study around citrus waste-derived limonene as a solvent for cleaning applications. Biofuels, Bioprod. Bioref., 10, 686-698. https://doi.org/10.1002/bbb.1677

64. Park, J. C., Lee, M. C., Yoon, D. S., Han, J., Kim, M., Hwang, U. K., ... & Lee, J. S. (2018). Effects of bisphenol A and its analogs bisphenol F and S on life parameters, antioxidant system, and response of defensome in the marine rotifer Brachionus koreanus. *Aquatic toxicology*, *199*, 21-29. https://doi.org/10.1016/j.aquatox.2018.03.024

65. Peng, X., Zheng, K., Liu, J., Fan, Y., Tang, C., & Xiong, S. (2018). Body size–dependent bioaccumulation, tissue distribution, and trophic and maternal transfer of phenolic endocrine-disrupting contaminants in a freshwater ecosystem. *Environmental toxicology and chemistry*, *37*(7), 1811-1823.

66. Perveen, S., Nadeem, R., Nosheen, F., Asjad, M. I., Awrejcewicz, J., & Anwar, T. (2022). Biochar-Mediated Zirconium Ferrite Nanocomposites for Tartrazine Dye Removal from Textile Wastewater. *Nanomaterials (Basel, Switzerland)*, *12*(16), 2828. https://doi.org/10.3390/nano12162828.

67. Pettinato, M., Chakraborty, S., Arafat, H. A., & Calabro', V. (2015). Eggshell: A green adsorbent for heavy metal removal in an MBR system. *Ecotoxicology and environmental safety*, *121*, 57–62. https://doi.org/10.1016/j.ecoenv.2015.05.046.

68. Rangabhashiyam, S., Lins, P. V. D. S., Oliveira, L. M. T. M., Sepulveda, P., Ighalo, J. O., Rajapaksha, A. U., & Meili, L. (2022). Sewage sludge-derived biochar for the adsorptive removal of wastewater pollutants: A critical review. *Environmental pollution (Barking, Essex : 1987)*, *293*, 118581. https://doi.org/10.1016/j.envpol.2021.118581.

69. Ravindran, R., & Jaiswal, A. K. (2016). Exploitation of Food Industry Waste for High-Value Products. *Trends in biotechnology*, *34*(1), 58–69. https://doi.org/10.1016/j.tibtech.2015.10.008.

70. Rio, S., Le Coq, L., Faur, C., Lecomte, D., & Le Cloirec, P. (2006). Preparation of adsorbents from sewage sludge by steam activation for industrial emission

treatment. *Process Safety and Environmental Protection*, *84*(4), 258-264. https://doi.org/10.1205/psep.05161

71. Rivas, B., Torrado, A., Torre, P., Converti, A., & Dominguez, J. M. (2008). Submerged citric acid fermentation on orange peel autohydrolysate. Journal of Agricultural and Food Chemistry, 56(7), 23280-2387.

72. Rivas, B., Torrado, A., Torre, P., Converti, A., & Dominguez, J. M. (2008). Submerged citric acid fermentation on orange peel autohydrolysate. Journal of Agricultural and Food Chemistry, 56(7), 23280-2387. doi:10.1021/jf073388r

73. Šafařík, I., Maděrová, Z., Pospíšková, K., Schmidt, H. P., Baldíková, E., Filip, J., Křížek, M., Malina, O., & Šafaříková, M. (2016). Magnetically modified biochar for organic xenobiotics removal. *Water science and technology : a journal of the International Association on Water Pollution Research*, *74*(7), 1706–1715. https://doi.org/10.2166/wst.2016.335.

74. Šafařík, I., Maděrová, Z., Pospíšková, K., Schmidt, H. P., Baldíková, E., Filip, J., Křížek, M., Malina, O., & Šafaříková, M. (2016). Magnetically modified biochar for organic xenobiotics removal. *Water science and technology : a journal of the International Association on Water Pollution Research*, *74*(7), 1706–1715. https://doi.org/10.2166/wst.2016.335.

75. Salaudeen, S. A., Tasnim, S. H., Heidari, M., Acharya, B., & Dutta, A. (2018). Eggshell as a potential CO_2 sorbent in the calcium looping gasification of biomass. *Waste management (New York, N.Y.)*, *80*, 274–284. https://doi.org/10.1016/j.wasman.2018.09.027.

76. Salgueiro-González, N., Turnes-Carou, I., Besada, V., Muniategui-Lorenzo, S., López-Mahía, P., & Prada-Rodríguez, D. (2015). Occurrence, distribution and bioaccumulation of

endocrine disrupting compounds in water, sediment and biota samples from a European river basin. *Science of the Total Environment*, *529*, 121-130.

77. Saputra, E., Zhang, H., Liu, Q., Sun, H., & Wang, S. (2016). Egg-shaped core/shell α-Mn2O3@α-MnO2 as heterogeneous catalysts for decomposition of phenolics in aqueous solutions. *Chemosphere*, *159*, 351–358. https://doi.org/10.1016/j.chemosphere.2016.06.021.

78. Schlagenhauf, L., Buerki-Thurnherr, T., Kuo, Y. Y., Wichser, A., Nüesch, F., Wick, P., & Wang, J. (2015). Carbon nanotubes released from an epoxy-based nanocomposite: quantification and particle toxicity. *Environmental science & technology*, *49*(17), 10616-10623. DOI: 10.1021/acs.est.5b02750

79. Schug, T. T., & Birnbaum, L. S. (2014). Human health effects of bisphenol A. *Toxicants in food packaging and household plastics: Exposure and health risks to consumers*, 1-29.

80. Shaikh, W. A., Kumar, A., Chakraborty, S., Islam, R. U., Bhattacharya, T., & Biswas, J. K. (2022). Biochar-based nanocomposite from waste tea leaf for toxic dye removal: From facile fabrication to functional fitness. *Chemosphere*, *291*(Pt 2), 132788. https://doi.org/10.1016/j.chemosphere.2021.132788.

81. Shang, B., Wang, S., Lu, L., Ma, H., Liu, A., Zupanic, A., Jiang, L., Elnawawy, A. S., & Yu, Y. (2022). Poultry eggshell-derived antimicrobial materials: Current status and future perspectives. *Journal of environmental management*, *314*, 115096. https://doi.org/10.1016/j.jenvman.2022.115096.

82. Singh, K. P., Malik, A., Sinha, S., & Ojha, P. (2008). Liquid-phase adsorption of phenols using activated carbons derived from agricultural waste material. *Journal of hazardous materials*, *150*(3), 626-641.

83. Sizmur, T., Fresno, T., Akgul, G., Frost, H., Jimenez, E.M. (2017). Biochar modification to enhance sorption of inorganics from water. Bioresource technology, 246, 34-37.

84. Tang, S., He, C., Thai, P. K., Heffernan, A., Vijayasarathy, S., Toms, L., ... & Mueller, J. F. (2020). Urinary concentrations of bisphenols in the Australian population and their association with the per capita mass loads in wastewater. *Environmental Science & Technology*, *54*(16), 10141-10148.

85. Tang, Y., Li, Y., Zhan, L., Wu, D., Zhang, S., Pang, R., & Xie, B. (2022). Removal of emerging contaminants (bisphenol A and antibiotics) from kitchen wastewater by alkali-modified Biochar. *Science of the Total Environment*, *805*, 150158.

86. Toles, C. A., Marshall, W. E., Johns, M. M., Wartelle, L. H., & McAloon, A. (2000). Acid-activated carbons from almond shells: physical, chemical and adsorptive properties and estimated cost of production. *Bioresource technology*, *71*(1), 87-92. https://doi.org/10.1016/S0960 -8524(99)00029-2

87. Tong, W., Xie, Y., Hu, W., Peng, Y., Liu, W., Li, Y., ... & Wang, Y. (2020). A bifunctional CoP/N-doped porous carbon composite derived from a single source precursor for bisphenol A removal. *RSC advances*, *10*(17), 9976-9984. https://doi.org/10.1016/S0960 -8524(99)00029-2

88. Torres-García, J. L., Ahuactzin-Pérez, M., Fernández, F. J., & Cortés-Espinosa, D. V. (2022). Bisphenol A in the environment and recent advances in biodegradation by fungi. *Chemosphere*, *303*, 134940.

89. Van Nguyen, T. T., Phan, A. N., Nguyen, T. A., Nguyen, T. K., Nguyen, S. T., Pugazhendhi, A., & Ky Phuong, H. H. (2022). Valorization of agriculture waste biomass as biochar: As first-rate biosorbent for remediation of contaminated soil. *Chemosphere*, *307*(Pt 3), 135834. https://doi.org/10.1016/j.chemosphere.2022.135834.

90. Veksha, A., Bhuiyan, T. I., & Hill, J. M. (2016). Activation of aspen wood with carbon dioxide and phosphoric acid for removal of total organic carbon from oil sands produced water: Increasing the yield with bio-oil recycling. *Materials*, *9*(1), 20. https://doi.org/10.3390/ma901 0020

91. Wang, J., & Wang, S. (2021). Toxicity changes of wastewater during various advanced oxidation processes treatment: An overview. *Journal of Cleaner Production*, *315*, 128202.

92. Wang, K., Peng, N., Sun, J., Lu, G., Chen, M., Deng, F., Dou, R., Nie, L., Zhong, Y. (2020). Synthesis of silica-composited biochars from alkali-fused fly ash and agricultural wastes for enhanced adsorption of methylene blue. Science of The Total Environment, 729, 139055. https://doi.org/10.1016/j.scitotenv.

93. Wang, Q., Chen, M., Shan, G., Chen, P., Cui, S., Yi, S., & Zhu, L. (2017). Bioaccumulation and biomagnification of emerging bisphenol analogues in aquatic organisms from Taihu Lake, China. *Science of the Total Environment*, *598*, 814-820.

94. Wang, Q., Li, J. S., & Poon, C. S. (2022). An iron-biochar composite from co-pyrolysis of incinerated sewage sludge ash and peanut shell for arsenic removal: Role of silica. *Environmental pollution (Barking, Essex : 1987)*, *313*, 120115. https://doi.org/10.1016/j.envpol.2022.120115.

95. Wang, Y., Dong, H., Li, L., Tian, R., Chen, J., Ning, Q., Wang, B., Tang, L., & Zeng, G. (2019). Influence of feedstocks and modification methods on biochar's capacity to activate hydrogen peroxide for tetracycline removal. *Bioresource technology*, *291*, 121840. https://doi.org/10.1016/j.biortech.2019.121840.

96. Xu, J., Hu, S., Min, L., & Wang, S. (2022). Waste eggshell-supported CuO used as heterogeneous catalyst for reactive blue 19 degradation through peroxymonosulfate activation (CuO/eggshell catalysts activate PMS to degrade reactive blue 19). *Water science*

and technology : a journal of the International Association on Water Pollution Research, *85*(11), 3271–3284. https://doi.org/10.2166/wst.2022.165.

97. Yoon, K., Cho, D. W., Bhatnagar, A., & Song, H. (2020). Adsorption of As(V) and Ni(II) by Fe-Biochar composite fabricated by co-pyrolysis of orange peel and red mud. *Environmental research*, *188*, 109809. https://doi.org/10.1016/j.envres.2020.109809.

98. Yu, C., Tang, J., Su, H., Huang, J., Liu, F., Wang, L., & Sun, H. (2022). Development of a novel biochar/iron oxide composite from green algae for bisphenol-A removal: adsorption and Fenton-like reaction. *Environmental Technology & Innovation*, *28*, 102647. https://doi.org/10.1016/j.eti.2022.102647.

99. Yu, F., Tian, F., Zou, H., Ye, Z., Peng, C., Huang, J., Zheng, Y., Zhang, Y., Yang, Y., Wei, X., Gao, B. (2021). ZnO/biochar nanocomposites via solvent free ball milling for enhanced adsorption and photocatalytic degradation of methylene blue. Journal of Hazardous Materials, 415, 125511. https://doi.org/10.1016/j.jhazmat.

100. Yu, J., Chang, J.S., Guo, H., Han, S., Lee, D.J. (2023). Sodium ions removal by sulfuric acid-modified biochars. Environmental Research, 235, 116592.

101. Zafar, F. F., Marrakchi, F., Barati, B., Yuan, C., Cao, B., & Wang, S. (2022). Highly efficient adsorption of Bisphenol A using NaHCO3/CO2 activated carbon composite derived from shrimp shell@ cellulose. *Environmental Science and Pollution Research*, *29*(45), 68724-68734. https://doi.org/10.1007/s11356-022-20564-9

102. Zhang, J., Gu, F., Zhou, Y., Li, Z., Cheng, H., Li, W., Ji, R., Zhang, L., Bian, Y., Han, J., Jiang, X., Song, Y., & Xue, J. (2022). Assisting the carbonization of biowaste with potassium formate to fabricate oxygen-doped porous biochar sorbents for removing organic pollutant from aqueous solution. *Bioresource technology*, *360*, 127546. https://doi.org/10.1016/j.biortech.2022.127546.

103. Zhang, J., Ji, H., Liu, Z., Zhang, L., Wang, Z., Guan, Y., & Gao, H. (2022). 3D Porous Structure-Inspired Lignocellulosic Biosorbent of *Medulla tetrapanacis* for Efficient Adsorption of Cationic Dyes. *Molecules (Basel, Switzerland)*, *27*(19), 6228. https://doi.org/10.3390/molecules27196228.

104. Zhang, M., Lin, K., Zhong, Y., Zhang, D., Ahmad, M., Yu, J., Fu, H., Xu, L., Wu, S., & Huang, L. (2022). Functionalizing biochar by Co-pyrolysis shaddock peel with red mud for removing acid orange 7 from water. *Environmental pollution (Barking, Essex : 1987)*, *299*, 118893. https://doi.org/10.1016/j.envpol.2022.118893.

105. Zhang, P., O'Connor, D., Wang, Y., Jiang, L., Xia, T., Wang, L., Tsang, D. C. W., Ok, Y. S., & Hou, D. (2020). A green biochar/iron oxide composite for methylene blue removal. *Journal of hazardous materials*, *384*, 121286. https://doi.org/10.1016/j.jhazmat.2019.121286.

106. Zhao, C., Wang, B., Theng, B. K. G., Wu, P., Liu, F., Wang, S., Lee, X., Chen, M., Li, L., & Zhang, X. (2021). Formation and mechanisms of nano-metal oxide-biochar composites for pollutants removal: A review. *The Science of the total environment*, *767*, 145305. https://doi.org/10.1016/j.scitotenv.2021.145305

107. Zhao, C., Wang, B., Theng, B. K., Wu, P., Liu, F., Wang, S., ... & Zhang, X. (2021). Formation and mechanisms of nano-metal oxide-biochar composites for pollutants removal: A review. *Science of the Total Environment*, *767*, 145305.

108. Zhao, L., Zheng, W., Masek, O., Chen, X., Gu, B., Sharma, B.K., & Cao, X. (2017). Roles of phosphoric acid in biochar formation: synchronously improving carbon retention and sorption capacity.

109. Zhao, X., Qiu, W., Zheng, Y., Xiong, J., Gao, C., & Hu, S. (2019). Occurrence, distribution, bioaccumulation, and ecological risk of bisphenol analogues, parabens and their metabolites in the Pearl River Estuary, South China. *Ecotoxicology and environmental safety*, *180*, 43-52.

110. Zhao, Z., Cao, Y., Li, S., & Zhang, Y. (2021). Effects of biowaste-derived biochar on the electron transport efficiency during anaerobic acid orange 7 removal. *Bioresource technology*, *320*,124295. https://doi.org/10.1016/j.biortech.2020.124295.

111. Zhu, F., Ma, S., Liu, T., & Deng, X. (2018). Green synthesis of nano zero-valent iron/Cu by green tea to remove hexavalent chromium from groundwater. *Journal of Cleaner Production*, *174*, 184-190.

VII Current research -publications

(1) Kumar, N., Vach, M., Saini, V.K., & Zitkova, A. (2024). Co-pyrolysis of orange peel and eggshell for oxygenated rich composite: Process optimization with response surface methodology. Journal of Environmental Management , 351 , 119786.